

Anonymous Referee #1

I find this manuscript much improved over the previous version. I appreciate that the authors responded actively to most of the critical comments that I made in my earlier review.

I am still worrying about the single case simulation to derive the conclusion. I would like to see the simulation results for other fog cases besides Tule fog case, because we do not know how the modified SOWC model simulates other fog cases under different meteorological condition and how the modified radiation scheme affects the fog formation. The authors just speculate the expected results as following (“Thus, for other fog cases the results might be different because the model can perform differently, better or worse, but we expect that the conclusion will be similar, if fog is successfully simulated”). However, I will leave the decision to the editor.

Reply: The authors appreciate the reviewer’s suggestions. We would very much like to extend our study to fog cases under different weather conditions over other regions to have a more robust conclusion on how aerosol mixing states affect fog formation and the radiation budget. However, to run a case at a different region requires a significant amount of effort. Aerosols in California have been carefully investigated using the SOWC model (Joe et al., 2014; Zhang et al., 2014). Thus the model gives more creditability to study a Tule fog event in California. While the WRF model has been well tested under different weather conditions over different regions in the world, we still need reliable emission data and reasonable air pollution simulations over a new region before we study a fog event there. Since the project ended, we do not have resources to extend the air pollution work over another region during a fog event. Without a careful study verifying that the emissions data support robust air pollution predictions over a new region using the SOWC model, we are very reluctant to draw conclusions about a fog case there. We are working to secure additional funding for these future studies, but they are beyond the scope of the current work. We have added a comment in the revised manuscript summary to reflect this. Lines 665-667.

”Note that the current results are based on a Tule fog case study in the Central Valley of California. Additional fog case studies under different weather conditions in other regions of the world are required to draw conclusions at those locations.”

Anonymous Referee #2

This paper investigates the effect of aerosol mixing state on fog formation by implementing warm-cloud processes in a source-oriented WRF/Chem model. With several model experiments, the authors make great efforts to show that the source-oriented representation of particles is a more realistic approach than the internal mixture approach for the study of direct, indirect, and semi-indirect effects of anthropogenic aerosols. The topic of the paper is definitely of crucial importance for studying aerosol–cloud–radiation interactions and for predicting the effects of climate change on the hydrological cycle and energy budget. However, the advantages of the source-oriented approach are not fully applied in this study although the results of aging processes are compared with those of internal mixing state assumption. The specific mechanism of aerosol influence on fog formation is not well investigated as it should be. Moreover, the model used in this study underestimated ammonium nitrate aerosols significantly, and the impacts on predicted hygroscopic properties of aerosols and thus CCN should have been investigated. The paper needs to be more concise and better written. Below are my detailed comments (for version2 of the manuscript), which need to be addressed before the paper can be considered for publication.

Reply: The authors appreciate the reviewer's comments. Follows are point-by-point response to the reviewer's comments. The bolded texts are added in the revised manuscript according to reviewer's comments.

Major comments:

1. Sect. 2.1, Sect. 2.2, Fig. 1 and Table 1: *The source-oriented representation of aerosol particles (AQC) as well as fog droplets (CLDAQC) is declared to be the core part of this study. However, whereas the AQC number concentrations are presented in Table 6, other sourced-oriented variables are not shown and actually none of the AQC and CLDAQC variables is given in the figures of this paper. In fact, the results of "source-oriented" simulations are not explicitly investigated in the paper. The "source-oriented" model appears not to be a fully suitable expression although it is frequently used in the paper; otherwise, more analyses of the source-oriented simulation results should be performed.*

The authors appreciate the reviewer's suggestion using "aging-process-included" instead of "sourced-oriented" to represent aerosol activation under near-realistic mixing condition in minor comment 4. We modified some phrases in the revised version to clarify the meaning. However, the term "source-oriented" is used in Zhang et al. (2014) to indicate the aerosol mixing state and chemistry presentation in the modified WRF/Chem model (i.e., the source-oriented WRF/Chem, SOWC, model). Since the current manuscript follows on to the studies from Zhang et al. (2014), we have retained the term "sourced-oriented" in the revised manuscript.

2. *The authors did several model experiments, as defined in Table 3, to investigate how aerosol mixing state influences fog formation. (a) However, they did not outlet clearly what are the specific mechanisms of aerosol influence on fog formation based on the above model results. (b) For the statement in Line 276-282, what are the other*

microphysical processes the authors mean? It would be very helpful if all the steps of aerosol-cloud-radiation interactions could be described here for clouds as well as for fogs. Please formulate the mechanism carefully for the model results and discussion.

(a) In the previous version of the manuscript, the discussion about how aerosol mixing state influences fog formation is scattered around Section 4.3. In this revised version, we provide a brief summary and discussion about how aerosol mixing state influences fog formation in the end of Section 4.3.

“In summary, compared to S_ARon_CRmod, I_ARon_CRmod has a higher CCN / cloud droplet number concentration because internally mixed aerosols can instantaneously contain hygroscopic material (e.g. sulfate) through artificial mixing, which decreases the critical supersaturation requirement for a particle to activate into a CCN, leading to higher cloud number concentration and optical thickness. Thicker fog in I_ARon_CRmod reduces the amount of shortwave radiation reaching the surface, resulting in a lower surface temperature. A lower surface temperature can have a positive feedback on cloud lifetime (i.e., a longer cloud lifetime), which further reduces shortwave radiation reaching the surface when compared to S_ARon_CRmod. Hence, the aerosols that include aging processes can delay CCN activation and produce fewer cloud droplets and less fog, which in turn will modify the energy budget near the surface.” in Lines 618-628.

(b) The brief concept of aerosol-cloud-radiation interactions has been introduced in the Introduction Section, Lines 70-76. In cloud microphysics, once aerosol particles activate as CCNs and become cloud droplets, they grow in size by diffusion initially. Later when droplets grow larger, autoconversion and collision/coalescence will occur to form rain droplets. If the ice phase (i.e., ice, snow, and graupel) exists, more microphysical processes will be involved, such as the Bergeron effect, riming, aggregation, melting, etc. Besides activation, the evaporation from rain droplets or melting from ice particles can contribute to the number of cloud droplets. We have modified the text to

“Fog is an excellent scientific case study that can isolate cloud activation and diffusive growth, the first step of aerosol-cloud-radiation interactions, from other microphysical processes that usually do not occur in fog, such as collision/coalescence, riming, melting, and aggregation. This paper presents the development of the CLDAQC treatment within the SOWC model to ensure that the model performs properly. A careful selection of a weather phenomenon is important to evaluate the model performance and the impact of the aerosol mixture states on cloud formation. The involvement of other hydrometeors, in addition to cloud droplets, can not only change the cloud properties and cloud lifetime, but also modify the energy budget. These extremely nonlinear processes can significantly complicate the evaluation of the model performance and the first step of aerosol-cloud-radiation interaction. Thus we choose fog as our very first weather system study for the evaluation of aerosol-cloud-radiation interactions using the improved SOWC model.” in Lines 276-287.

3. In the S_ARon_CRmod scheme, the cloud droplets are allowed to range in size from dry aerosol particle radius to 30 microns when calculating the cloud optical thickness (Line 479-480). This setting is likely to result in errors when calculating the cloud optical thickness, because cloud droplet radius is usually greater than 1

microns and thus unacted particles are involved in the calculation. Please state clearly the reasons for this setting.

The sentence that we wrote was misleading and we have clarified the description in the revised version. We do not include unactivated aerosols in the calculation of cloud optical thickness (COT). In the modified radiation scheme (e.g., S_ARon_CRmod), cloud droplet size varies for each bin and source types. In the original radiation scheme, the effective radius (r_e) is diagnosed assuming a constant radius which is capped within a range ($4 \mu\text{m} \leq r_e \leq 20 \mu\text{m}$). In our modified code, we use simulated cloud radii to directly calculate COT and dry aerosol radii are only used for the lower bound of cloud droplet sizes to avoid numerical error (i.e. division by zero). Our calculation of the COT includes cloud droplets of all sizes (even very small ones), but the COT calculation does not include unactivated aerosols. We have modified the sentence to **“In the modified cloud-radiation scheme (CRmod), the size range of cloud droplets in Eq. (3) can vary between activated CCNs to 30 μm .”** in Lines 362-364.

4. As described in Line 483 and later on in the paper, the simulation results of optical thickness between S_ARon_CRmod and S_ARon_CRorig are very similar. The authors think “because the meteorological conditions of the fog event are calm and stable, the cloud microphysics processes are fairly slow and simple (no rain produced in this case)”. However, from the simulations of mean values of cloud liquid water (NOT mixing ratio as stated in the paper) and cloud droplet number (Table 5), one can see that the cloud water mixing ratios are similar, but the cloud droplet number concentrations are quite different, which means that the mean cloud droplet sizes should be different between the two experiments. Cloud droplet number concentration, cloud droplet size and cloud droplet index of refraction are the factors that can affect the calculation results of cloud optical thickness. So the authors need to synthesize the above-mentioned factors, and give the specific reasons for the simulation results.

This is a good question. We have described the differences of the cloud optical thickness calculation between S_ARon_CRorig and S_CRon_CRmod in response to reviewer’s comments in the previous revision. Since more than one reviewer has raised the same question, we have added the following in Lines 496-508 of the revised version.

“In the original radiation scheme, the cloud optical thickness (COT) is a function of cloud water path (CWP) and an effective radius ($4 \mu\text{m} \leq r_e \leq 20 \mu\text{m}$), which is derived from the water mass and the total droplet number assuming a uniform size of cloud droplets:

$$\tau_{orig}(\lambda) = CWP \times \left(-6.59 \times 10^{-3} + \frac{1.65}{r_e}\right). \quad (6)$$

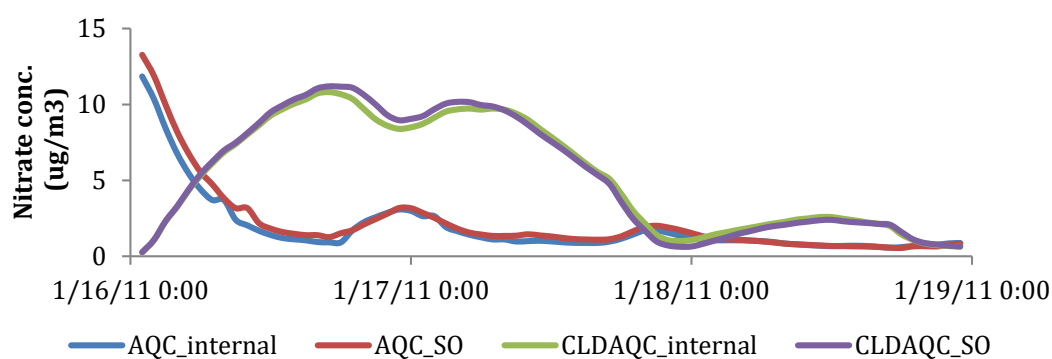
In the modified radiation scheme in S_ARon_CRmod, the COT is calculated based on simulated cloud droplet size, number, and chemical composition of each bin and source (Eq. 3). In addition, the formula of COT, single scattering albedo and asymmetry factor in the modified radiation scheme are all modified. With a similar Q_c , although Q_n in S_ARon_CRorig is higher than that in S_ARon_CRmod, the COT is slightly higher in S_ARon_CRmod due to different formulas used in the calculation of cloud-radiation interaction. The small

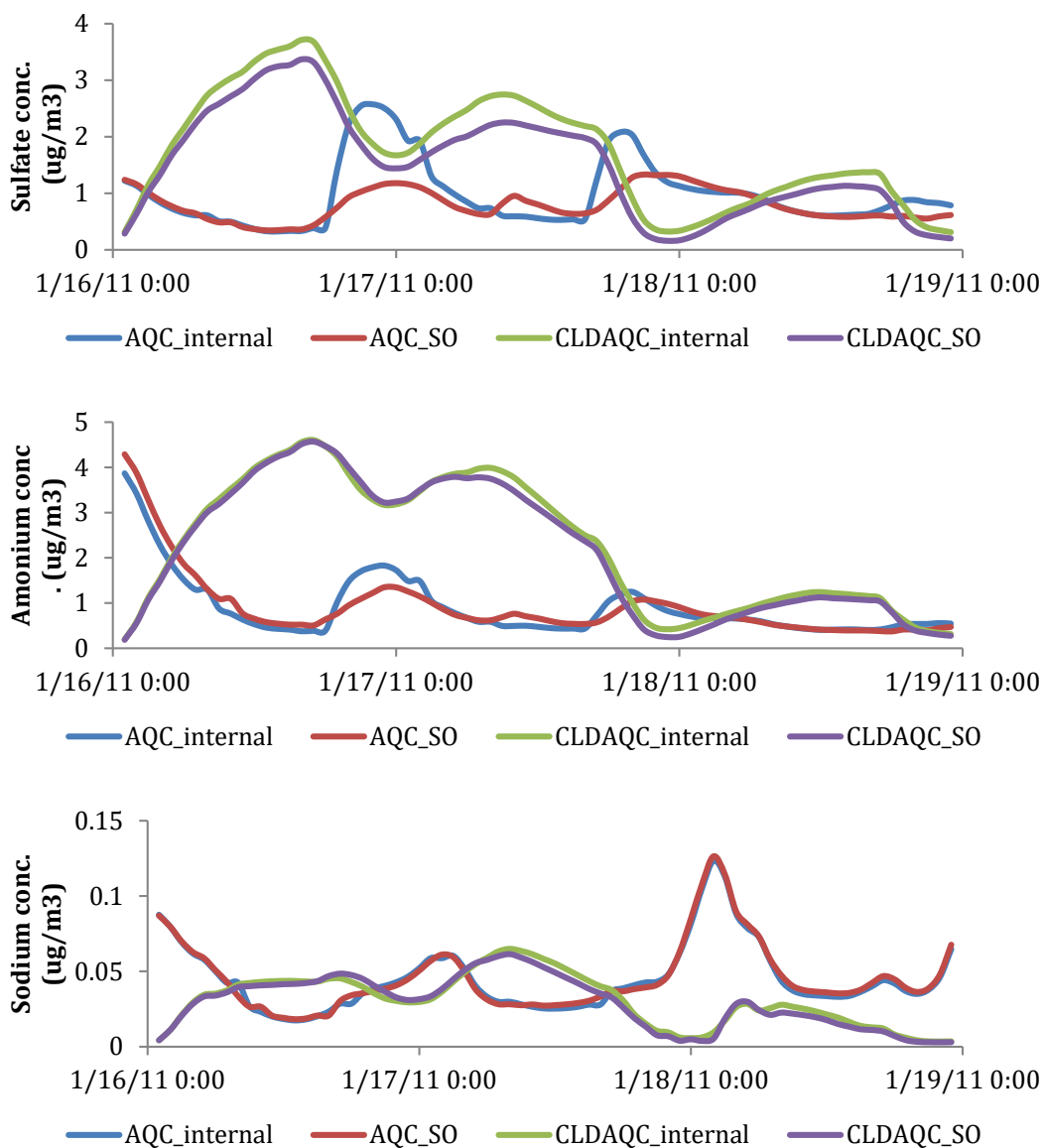
difference of COT between these two experiments in fact indicates that the parameterization of COT in the original radiation scheme provides a reasonable result compared to the explicit COT calculation.“

We thank the reviewer pointing out the incorrect use of the term “cloud water mixing ratio”. We correct the term to “cloud liquid water” in the revised version.

5. As described in Sect. 4.1 of the paper (Line 399-412), both simulated nitrate and ammonium concentrations are underestimated by 70%. This implies that ammonium nitrate, which has a great potential of absorbing water molecules, is significantly underestimated. What effects of such poor behavior of the model on the size distributions and hygroscopic properties of aerosols, CCN and fog formation? It would not be advised if the reader is merely referred to a paper of Zhang et al. (2014) without providing the cause of discrepancy and the effects on fog simulation.

The nitrate under-prediction is not unusual in reactive chemical transport models (e.g., WRF/Chem and CMAQ; see for example peak nitrate under-predictions in Fig 6 of Kelly et al. (2014)). There are numerous current research projects underway to identify and correct the cause of this problem. We had hoped that feedbacks between meteorology and atmospheric chemistry were part of the answer and that is the hypothesis that was tested in the current study. Unfortunately, the feedbacks do not seem to increase predicted nitrate formation, and so we must rely on results from other projects to address this point. However, based on the time series of chemical concentration in aerosols (AQC) and cloud (CLDAQC) in S_ARon_CRmod and I_ARon_CRmod (figures below), the model well simulated nucleation process for four species. Although we do not know whether the Nitrate and Ammonium concentration were underestimated before the fog formed, our model did correctly simulate aerosol activation processes and the concentration of those chemical species can be tracked in both aerosols (AQC) and cloud (CLDAQC). Nitrate and Ammonium were under-predicted after fog dissipation on 18 January because most Ammonium and Nitrate are released back to the gas phase. This potentially explains why Nitrate and Ammonium are significantly underestimated in the condensed phase (Fig. 6 in the manuscript). Unfortunately, we only have observations on the last day of simulation (18th) when fog almost dissipated. With this limited observations, it is difficult to effectively evaluate the cause of the underestimation of Nitrate and Ammonium.





Minor comments:

1) Line 90-93: In fact, the aging timescale was investigated previously based on aircraft measurements, e.g., in the work of Ma et al. (2010). Ma et al. (2010) showed that the coating of dust particles by high pollution acids (due to high emission rates of their precursors) is very efficient with a timescale of a few hours, providing the predominant source of CCN, and such coating is more efficient with increasing OH (which is a measure of the oxidation capacity of the atmosphere). Therefore, instead of stating that little information is available, such kind of work should be cited in the paper.

The authors thank the reviewer for providing the useful information and suggestion. We have modified the text to **“From the IPAC-NC (Influence of Pollution on Aerosols and Cloud Microphysics in North China) field campaign data, Ma et al. (2010) showed that dust particles can become the predominant source of CCNs in a few hours after being coated by high pollution acids. This aging process has**

been parameterized in numerical models (Lesins et al., 2002) but how the aging timescale should respond to changes in temperature, humidity, oxidant concentrations and/or emissions rates is not described in most models.” in Lines 104-110.

2) *Line 107-113 and Line 163-164: Does the model include new particle formation processes? It looks that the new nucleation mode (typically for particle sizes less than 25 nm) is not taken into account in both the schemes. It is stated that the particle size of first bin from emissions is 5 nm, which appears too small compared to the size of the first bin (39 nm) the model scheme has considered.*

The authors thank the reviewer to point out the typo in the manuscript. The particle size of the first bin in our model is 55 nm, not 5 nm. Both MADE-SORGAM and MOSAIC aerosol schemes in the WRF/Chem include new particle formation processes and so does SOWC but these processes were not active in the current simulations. The San Joaquin Valley is one of the most heavily polluted air basins in the United States with relatively large concentrations of primary particles but at the same time relatively low emissions of SO₂ due to emissions control programs that limit the sulfur content of fuel. Under these conditions, nucleation of new particles is a minor process compared to emissions and atmospheric processing of primary particles. The current manuscript focuses on these mechanisms, and defers the discussion of nucleation to a future study in a location where this process is important for CCN formation.

3) *Line 178-193: There are several cloud schemes in WRF-Chem, such as Morrison scheme. Why do the authors select Purdue Lin scheme, and do you have verify the simulation capability of the scheme?*

The Purdue Lin scheme was developed at Purdue University and was published by the second author of the manuscript and her advisor (Chen and Sun, 2002). Thus we are very familiar with the scheme and the code. The scheme has been used in many studies (Cruz and Narisma, 2016; Anber et al., 2016; and many others). Although the original Purdue Lin scheme is a one-moment scheme, Chapman et al. (2009) added a prognostic treatment of cloud droplet number to the scheme to make it a two-moment scheme on cloud water within WRF/Chem. This is the first scheme in the WRF model that considers the aerosol-cloud interaction (CCN). From the reasons mentioned above, we therefore chose this scheme for the study.

4) *Line 280: It might be more suitable to use a phrase like “aging-process-included” to replace the “source-oriented” here, as the basic chemical and physical processes for fog formation are the same no matter whether the sources are tagged or not.*

We agree that using “aging-process-included” instead of “sourced-oriented” in this sentence is more appropriate to represent aerosol activation under near-realistic mixing condition. We have modified this instance and similar instances of the phrase throughout the revised manuscript to clarify the meaning. Again, the term “source-oriented” is used in Zhang et al. (2014) to indicate our new modified treatment of aerosol chemistry mixing state in the model (the source-oriented WRF/Chem, SOWC). Since this manuscript follows on to the studies by Zhang et al., we prefer to retain the term “source-oriented” in appropriate locations throughout the manuscript.

5) Line 282: *What instruments were used to measure surface relative humidity? Could the fog formation take place below RH=100% in the Central Valley (see e.g. Kulmala et al., 1997; Makkonen et al., 2012)? By using what parameters and their threshold values is a fog event identified to occur in this study?*

A hygrometer is an instrument used to measure relative humidity in most ground-based weather stations, which belong to National Weather Service. Based on reviewer's suggestion, we have added **“For example, the IPAC-NC field campaign in China observed clouds formed in a polluted environment with RH below 100% due to high hygroscopic pollutants (Ma et al., 2010).”** in Lines 293-294.

RH measurements were just one of the parameters used to select the current case for study with the SOWC model. We also used geostationary satellite images as another observation of fog conditions. Due to some high hygroscopic pollutants (e.g., Nitrate) formed in the Central Valley, we believe it may be possible that Tule fog can form when RH is below 100%, though we do not have data to verify.

6) Line 416-417: *What causes are for such an underestimation of LWP? Could this be linked to an underestimation of ammonium nitrate?*

The cause for the underestimation of LWP in the middle portion of the Central Valley is not clear. The third author has different projects working on this research area. However, as we described above, underestimated Nitrate and Ammonium is probably a consequence of fog formation (i.e., released back to the gas phase after evaporation) in this study.

7) Line 466-467: *How or by what processes does the aerosol direct effect lead to increases of the cloud water mass and cloud droplet number?*

Aerosol particles absorb and scatter shortwave radiation, leading to a smaller shortwave flux reaching the surface. In our study, Table 5 shows that the average NSF within the Central Valley from S_ARoff_CRmod is higher than from S_ARon_CRmod by 3.7 W m^{-2} . This means that the aerosol direct radiative forcing reduces an average of the shortwave energy flux on the ground by 3.7 W m^{-2} and thus produces a lower skin temperature in this case study. A lower skin temperature (0.1 K) provides a favorable condition for cloud/fog formation near the surface. Compared to S_ARoff_CRmod, the mean values of cloud liquid water and cloud droplet number are increased by 3.3% and 4.5%, respectively, in S_ARon_CRmod (Table 5).

8) *There have been some studies about the effect of aerosol mixing state on CCN and warm cloud formation before this work. The author should refer to the literatures during their analysis and discussion (e.g., Cubison et al., 2008; Lance et al., 2013; Anttila et al., 2010;).*

We have added the following in the Introduction Section of the revised manuscript.

“Some studies showed the importance of the aerosol mixing state on CCN activation using field campaign data and numerical modeling. Cubison et al. (2008) focused on the relationship between the CCN number concentration and

the physical and chemical properties of aerosols in the urban area in California. Based on the results from a cloud parcel model and observed CCN number, they found that a realistic treatment of the mixing state of the urban aerosol distribution is critical to the CCN activation prediction. Anttila (2010) also used an adiabatic cloud parcel model to investigate the importance of the particle mixing state and hygroscopicity to CCN activation. They commented that the differences between externally and internally mixed aerosols in urban and rural environments could reach up to 35%. Both modeling studies investigated the effect of aerosol mixing state on CCN formation based on an ideal cloud parcel model. While observations from Ma et al. (2010) and Lance et al. (2013) showed consistent results with these modeled CCN studies, a more sophisticated 3-dimensional numerical model is needed to further study this issue.” in Lines 88-101.

Technical issues:

Line 430-431: Smaller cloud droplets are not shown in the figure.

Observed LWP and modeled LWP are comparable with one-day shift (Fig. 7). Based on Eq. (3), to obtain a higher cloud optical thickness one expects to have a higher number concentration with smaller cloud droplets in order to maintain a comparable LWP. We have rewritten the sentence to clarify this point.

“While simulated LWP is comparable to MODIS retrievals with one-day shift (Fig. 7), to obtain a higher COT than observed (Fig. 8b versus 8c) we expect that the model produces more small cloud droplets with a higher CCN concentration, especially over highly polluted areas.” in Lines 449-451.

Formulas (2)-(5), Tables 4 and 5: Same character Q is used for different variables though having different subscripts.

Q_e , Q_s , Q_2 , Q_c , and Q_n are the dimensionless extinction efficiency, the dimensionless scattering efficiency, 2-m water vapor mixing ratio, cloud liquid water, and cloud droplet number, respectively. Q always has a subscript and should therefore be clear to the reader.

Line 463, 574, 589: Should “water mixing ratio” be a dimensionless variable or it should be called water content?

We corrected “cloud water mixing ratio” to “cloud liquid water” in the revised version.

Line 544-545: Can one learn hydrophobic nature of particles from Table 6?

We have modified the sentences to **“Most particles tracked in the AQC size bin 1 can activate in the internally mixed experiment; however, in the source-oriented experiment only particles emitted in AQC size bin 1 from wood smoke and “other sources” are sufficiently hygroscopic to activate. The remaining sources are dominated by hydrophobic compounds (such as elemental carbon) that do not activate under the study conditions (Table 6).”** in Lines 564-568.

Line 555-557: How one can see the changes after late 17 January from Table 4 that shows only mean values over 16-18 January?

Figure 9 shows time series of mean bias variation of 2-m temperature, 2-m vapor mixing ratio, and NSF from different experiments. Thus we revised the sentence to state “**After late 17 January, the bias differences between two experiments are more apparent in the daytime than in the nighttime (Fig. 9 and Table 4).**” in Lines 558-559.

Line 617: better to use important “results”, instead of “findings”.

Modified.

Table 1: not fully useful.

Table 1 was added based on another reviewer’s comment to provide the aerosol chemistry information for readers. We prefer to retain the table based on that original reviewer suggestion.

Table 6: What does the Ratio mean? Information on particle size ranges of each bin can be provided.

The ratio is the aerosol concentration for each bin/source divided by the total. This has been clarified in the caption of Table 6. The size range for each AQC bin (S_ARon_CRmod) is now added in the supplementary.

“Table 6. The ratio of AQC number concentration for each bin/source to the total number concentration. The numbers are averaged within the first five model layers during 16 to 18 January 2011.”

(Units in μm)

bin1	0.058	~	0.069
bin2	0.122	~	0.139
bin3	0.239	~	0.260
bin4	0.480	~	0.507
bin5	0.874	~	1.070
bin6	0.914	~	1.886
bin7	2.633	~	4.541
bin8	5.695	~	10.844

Line 1091 (Fig. 7 legend): should be (b), (d) and (f).

Corrected.

Line 1123 (Fig. 10): At what supersaturation?

It is real ratio of activated CCN number to existing aerosol number. So the supersaturation varies at each grid point.

Line 1154 (Fig. 13): better be plotted in colour.

Changed.

References:

- Anber, U., Wang, S., and Sobel, A.: Response of Atmospheric Convection to Vertical Wind Shear: Cloud-System-Resolving Simulations with Parameterized Large-Scale Circulation. Part II: Effect of Interactive Radiation, *Journal of the Atmospheric Sciences*, 73, 199-209, doi:10.1175/JAS-D-15-0151.1, 2016.
- Chapman, E. G., Gustafson Jr, W. I., Easter, R. C., Barnard, J. C., Ghan, S. J., Pekour, M. S., and Fast, J. D.: Coupling aerosol-cloud-radiative processes in the WRF-Chem model: Investigating the radiative impact of elevated point sources, *Atmos. Chem. Phys.*, 9, 945-964, 10.5194/acp-9-945-2009, 2009.
- Chen, S.-H., and Sun, W.-Y.: A One-dimensional Time Dependent Cloud Model, *Journal of the Meteorological Society of Japan. Ser. II*, 80, 99-118, 10.2151/jmsj.80.99, 2002.
- Cruz, F. T., and Narisma, G. T.: WRF simulation of the heavy rainfall over Metropolitan Manila, Philippines during tropical cyclone Ketsana: a sensitivity study, *Meteorology and Atmospheric Physics*, 1-14, 10.1007/s00703-015-0425-x, 2016.
- Joe, D. K., Zhang, H., DeNero, S. P., Lee, H.-H., Chen, S.-H., McDonald, B. C., Harley, R. A., and Kleeman, M. J.: Implementation of a high-resolution Source-Oriented WRF/Chem model at the Port of Oakland, *Atmospheric Environment*, 82, 351-363, <http://dx.doi.org/10.1016/j.atmosenv.2013.09.055>, 2014.
- Kelly, J. T., Baker, K. R., Nowak, J. B., Murphy, J. G., Markovic, M. Z., VandenBoer, T. C., Ellis, R. A., Neuman, J. A., Weber, R. J., Roberts, J. M., Veres, P. R., de Gouw, J. A., Beaver, M. R., Newman, S., and Misenis, C.: Fine-scale simulation of ammonium and nitrate over the South Coast Air Basin and San Joaquin Valley of California during CalNex-2010, *Journal of Geophysical Research: Atmospheres*, 119, 3600-3614, 10.1002/2013JD021290, 2014.
- Lesins, G., Chylek, P., and Lohmann, U.: A study of internal and external mixing scenarios and its effect on aerosol optical properties and direct radiative forcing, *Journal of Geophysical Research-Atmospheres*, 107, 10.1029/2001jd000973, 2002.
- Zhang, H., DeNero, S. P., Joe, D. K., Lee, H. H., Chen, S. H., Michalakes, J., and Kleeman, M. J.: Development of a source oriented version of the WRF/Chem model and its application to the California regional PM₁₀ / PM_{2.5} air quality study, *Atmos. Chem. Phys.*, 14, 485-503, 10.5194/acp-14-485-2014, 2014.

1
2
3
4
5
6
7
8
9
10
11
12
13
14
15
16
17
18
19
20
21
22
23
24
25
26
27
28
29
30
31

**Implementation of Warm-Cloud Processes in a Source-Oriented
WRF/Chem Model to Study the Effect of Aerosol Mixing State on Fog
Formation in the Central Valley of California**

Hsiang-He Lee^{1*}, Shu-Hua Chen^{1@}, Michael J. Kleeman², Hongliang Zhang², Steven P.
DeNero², and David K. Joe²

¹ Department of Land, Air, and Water Resources, University of California, Davis, CA

² Department of Civil & Environmental Engineering, University of California, Davis, CA

Submitted to
Atmospheric Chemistry and Physics

October 18, 2015

[@]Corresponding author address: Dr. Shu-Hua Chen, Department of Land, Air, and Water
Resources, University of California, Davis, California 95616-8627.
E-mail: shachen@ucdavis.edu

^{*}now at: Singapore-MIT Alliance for Research and Technology (SMART), Centre for
Environmental Sensing and Modeling (CENSAM), Singapore

32

Abstract

33 The source-oriented Weather Research and Forecasting chemistry model (SOWC) was
34 modified to include warm cloud processes and applied to investigate how aerosol mixing
35 states influence fog formation and optical properties in the atmosphere. SOWC tracks a 6-
36 dimensional chemical variable (X, Z, Y, Size Bins, Source Types, Species) through an
37 explicit simulation of atmospheric chemistry and physics. A source-oriented cloud
38 condensation nuclei module was implemented into the SOWC model to simulate warm
39 clouds using the modified two-moment Purdue Lin microphysics scheme. The Goddard
40 shortwave and longwave radiation schemes were modified to interact with source-oriented
41 aerosols and cloud droplets so that aerosol direct and indirect effects could be studied.

42 The enhanced SOWC model was applied to study a fog event that occurred on 17
43 January 2011, in the Central Valley of California. Tule fog occurred because an atmospheric
44 river effectively advected high moisture into the Central Valley and nighttime drainage flow
45 brought cold air from mountains into the valley. The SOWC model produced reasonable
46 liquid water path, spatial distribution and duration of fog events. The inclusion of aerosol-
47 radiation interaction only slightly modified simulation results since cloud optical thickness
48 dominated the radiation budget in fog events. The source-oriented mixture representation of
49 particles reduced cloud droplet number relative to the internal mixture approach that
50 artificially coats hydrophobic particles with hygroscopic components. The fraction of
51 aerosols activating into CCN at a supersaturation of 0.5% in the Central Valley decreased
52 from 94% in the internal mixture model to 80% in the source-oriented model. This increased
53 surface energy flux by 3-5 W m⁻² and surface temperature by as much as 0.25 K in the
54 daytime.

55 **1. Introduction**

56 Atmospheric aerosols are complex mixtures of particles emitted from many different
57 anthropogenic and natural sources suspended in the atmosphere. In contrast to greenhouse
58 gases, aerosols have large spatial and temporal variability in the troposphere because of their
59 short lifetimes (about one week) before coagulation, dry deposition, or wet scavenging
60 processes remove them from the atmosphere (Ramanathan et al., 2001). Aerosol particles
61 can influence human health (McMichael et al., 2006), ecological health (over land and ocean)
62 (Griffin et al., 2001), visible range through the atmosphere, cloud / precipitation formation
63 (Chen et al., 2008), and the net radiation budget of the earth (IPCC, 2007). Some chemical
64 components of aerosol particles are important to direct radiative forcing of the climate due to
65 their optical properties (Tegen et al., 1996). Particulate sulfate scatters incoming solar
66 radiation, leading to an estimated direct forcing of -0.95 W m^{-2} (Adams et al., 2001).
67 Particulate black carbon strongly absorbs incoming shortwave radiation, which warms the
68 mid-level of the atmosphere but cools the earth's surface (Yang et al., 2009; Koch and Del
69 Genio, 2010). Particulate black carbon also leads to reduce relative humidity and cloud
70 liquid water content (semi-direct effect) in the mid-level atmosphere (Ackerman et al., 2000;
71 Koch and Del Genio, 2010). In addition to these direct effects, Twomey (1974) proposed
72 that aerosols indirectly affect the earth's energy budget due to their ability to serve as cloud
73 condensation nuclei (CCN), which are of great importance in cloud development, especially
74 for warm clouds in the mid-to-high latitudes. Large numbers of CCN produce clouds with a
75 greater number of smaller size cloud droplets (Chen et al., 2008). These smaller cloud
76 droplets raise cloud albedo (the first indirect effect) and also suppress the formation of
77 precipitation and prolong cloud lifetime (the second indirect effect) (Albrecht, 1989). The
78 direct, semi-direct, and indirect effects of aerosol particles modify the energy budgets in the
79 atmosphere and on the surface, with corresponding changes in atmospheric stability. The

80 2007 IPCC report (IPCC, 2007) concluded that the net forcing of all aerosols could be either
81 positive or negative in the range from -0.7 W m^{-2} to $+0.1 \text{ W m}^{-2}$. The majority of this
82 uncertainty is associated with the semi-direct and indirect effects due to the complexity of
83 aerosol-cloud interactions.

84 The magnitude of the aerosol semi-direct and indirect effects depends on the number
85 concentration, size, and composition of the atmospheric aerosol particles that act as CCN or
86 ice nuclei (IN) (Lohmann and Feichter, 2005; Chen et al., 2008). Particles with hygroscopic
87 components such as water-soluble ions (Na^+ , Cl^- , SO_4^{2-} , NO_3^- etc.) readily act as CCN (Chen
88 and Lamb, 1994). Particles that contain hydrophobic components such as freshly emitted
89 organic carbon or elemental carbon must become coated with hygroscopic material before
90 they will easily serve as CCN (Dusek et al., 2006). ~~This aging process is often parameterized
91 in models (Lesins et al., 2002) but little information is available to describe how the aging
92 timescale should respond to changes in temperature, humidity, oxidant concentrations and/or
93 emissions rates. Mineral dust particles (Motoi, 1951; Georgii and Kleinjung, 1967)
94 commonly have a favorable arrangement of surface structure that allows them to serve as IN.
95 Secondary coatings that condense on mineral dust particles may reduce their ability to serve
96 as IN (Sullivan et al., 2010) but increase their ability to serve as CCN (Li and Shao, 2009).
97 All of these effects. Some studies showed the importance of the aerosol mixing state on CCN
98 activation using field campaign data and numerical modeling. Cubison et al. (2008) focused
99 on the relationship between the CCN number concentration and the physical and chemical
100 properties of aerosols in the urban area in California. Based on the results from a cloud
101 parcel model and observed CCN number, they found that a realistic treatment of the mixing
102 state of the urban aerosol distribution is critical to the CCN activation prediction. Anttila
103 (2010) also used an adiabatic cloud parcel model to investigate the importance of the particle
104 mixing state and hygroscopicity to CCN activation. They commented that the differences~~

105 between externally and internally mixed aerosols in urban and rural environments could
106 reach up to 35%. Both modeling studies investigated the effect of aerosol mixing state on
107 CCN formation based on an ideal cloud parcel model. While observations from Ma et al.
108 (2010) and Lance et al. (2013) showed consistent results with these modeled CCN studies, a
109 more sophisticated 3-dimensional numerical model is needed to further study this issue.
110 Mineral dust particles (Motoi, 1951; Georgii and Kleinjung, 1967) commonly have a
111 favorable arrangement of surface structure that allows them to serve as IN. Secondary
112 coatings that condense on mineral dust particles may reduce their ability to serve as IN
113 (Sullivan et al., 2010) but increase their ability to serve as CCN (Li and Shao, 2009). From
114 the IPAC-NC (Influence of Pollution on Aerosols and Cloud Microphysics in North China)
115 field campaign data, Ma et al. (2010) showed that dust particles can become the predominant
116 source of CCNs in a few hours after being coated by high pollution acids. This aging process
117 has been parameterized in numerical models (Lesins et al., 2002) but how the aging timescale
118 should respond to changes in temperature, humidity, oxidant concentrations and/or emissions
119 rates is not described in most models. All of these mentioned above point to the importance
120 of the particle mixing state when predicting CCN / IN concentrations.

121 The standard Weather Research and Forecasting (WRF) model, including the chemistry
122 component (WRF/Chem), permits the simulation of the combined direct, indirect and semi-
123 direct effects of aerosols (Chapman et al., 2009; Fast et al., 2006; Grell et al., 2005).
124 WRF/Chem Version 3.1.1 has sophisticated packages to represent chemistry processes (i.e.
125 gas-phase reaction, gas-to-particle conversion, coagulation, etc.) and aerosol size and
126 composition (Zaveri et al., 2008; Ackermann et al., 1998; Binkowski and Shankar, 1995;
127 Schell et al., 2001). ~~The Modal Aerosol Dynamics Model for Europe with Secondary~~
128 ~~Organic Aerosol Model (MADE-SORGAM) and the Model for Simulating Aerosol~~
129 ~~Interactions and Chemistry (MOSAIC) are commonly used aerosol schemes in the~~

130 ~~WRF/Chem model. Both schemes have inorganic, organic, and secondary organic aerosols~~
131 ~~and contain aerosol formation processes including nucleation, condensation, and coagulation.~~
132 ~~The main difference between MADE-SORGAM and MOSAIC is the representation of~~
133 ~~aerosol size distributions. MADE-SORGAM uses 3 log-normal modes (Aitken,~~
134 ~~accumulation and coarse) while MOSAIC uses 4 (or 8) aerosol size sections (bins) from 39~~
135 ~~nm to 10 μ m, respectively. The details of MADE-SORGAM are described in Binkowski and~~
136 ~~Shankar (1995), Ackermann et al. (1998), Schell et al. (2001), and Grell et al. (2005) and the~~
137 ~~details of MOSAIC are given in Zaveri et al. (2008).~~

138 As mentioned above, the size, composition, and mixing state of aerosols strongly affect
139 their ability to activate into cloud droplets. The Modal Aerosol Dynamics Model for Europe
140 with Secondary Organic Aerosol Model (MADE-SORGAM) and the Model for Simulating
141 Aerosol Interactions and Chemistry (MOSAIC) are commonly used aerosol schemes in the
142 WRF/Chem model. Both schemes have inorganic, organic, and secondary organic aerosols
143 and contain aerosol formation processes including nucleation, condensation, and coagulation.
144 The main difference between MADE-SORGAM and MOSAIC is the representation of
145 aerosol size distributions. MADE-SORGAM uses 3 log-normal modes (Aitken,
146 accumulation and coarse) while MOSAIC uses 4 (or 8) aerosol size sections (bins) from 39
147 nm to 10 μ m, respectively. The details of MADE-SORGAM are described in Binkowski and
148 Shankar (1995), Ackermann et al. (1998), Schell et al. (2001), and Grell et al. (2005) and the
149 details of MOSAIC are given in Zaveri et al. (2008).

150 As mentioned above, the size, composition, and mixing state of aerosols strongly affect
151 their ability to activate into cloud droplets (Lance et al., 2013; Zaveri et al., 2010). However,
152 most WRF/Chem chemistry packages make a global internal mixing assumption in which all
153 particles within a log-normal mode (MADE-SORGAM) / size bin (MOSAIC scheme) in the

154 same grid cell are instantaneously combined such that they have the same chemical
155 composition. In reality, airborne particles are emitted with unique chemical composition and
156 only become internally mixed over a period of hours to days depending on atmospheric
157 conditions. The instantaneous internal mixing assumption alters the optical and chemical
158 properties of particles in WRF/Chem simulations (Zhang et al., 2014) and therefore has the
159 potential to influence aerosol-cloud interaction (i.e. CCN activation).

160 The primary goal of this research is to quantify the effect of assumptions about particle
161 mixing state on predicted cloud droplet formation within the WRF/Chem model. Warm
162 cloud processes in the Purdue Lin scheme (Chen and Sun, 2002) were modified in the
163 Source-Oriented WRF/Chem (SOWC) model to investigate the impact of aerosol mixing
164 state on the characteristics of a fog event in the Central Valley of California. The SOWC
165 model explicitly predicts particle mixing state in the presence of emissions, transport,
166 coagulation, chemical transformation, and deposition. The integration of warm-cloud
167 processes with the source-oriented treatment of particles in the current study provides a more
168 realistic approach to understand how mixing state influences direct, indirect, and semi-
169 indirect effects of anthropogenic aerosols.

170 This paper is organized as follows: the model description and development of warm
171 cloud processes are introduced in section 2; observational data and numerical experiment
172 design are presented in section 3; results are discussed in section 4; and the summary and
173 discussion are provided in section 5.

174 **2. Model Description and Development**

175 **2.1 SOWC**

176 WRF is a compressible, non-hydrostatic regional meteorology model, which uses the
177 Arakawa C grid and terrain-following hydrostatic pressure coordinates. The governing

178 equations of the model are written in flux form and can be solved using a range of solution
179 schemes. In the present study, the Runge-Kutta third-order time scheme was employed and
180 fifth- and third-order advection schemes were chosen for the horizontal and vertical
181 directions, respectively (Skamarock et al., 2008). WRF/Chem simulates trace gas and
182 particle chemical concentrations concurrently with the meteorological fields using the same
183 grid structure, the same advection scheme, and the same physics schemes for sub-grid scale
184 transport (Grell et al., 2005). The SOWC model was developed based on WRF/Chem V3.1.1
185 with significant modifications throughout the code to enable the use of 6D variables. The
186 standard WRF/Chem model tracks 3-dimensional chemistries in a 4-dimensional variable
187 (X, Z, Y, Species). The SOWC model tracks a 6-dimensional chemical variable “AQC” (X,
188 Z, Y, Size Bins, Source Types, Species). Particles emitted from different sources have
189 different sizes and chemical compositions, leading to a source-oriented mixture of particles
190 that age in the atmosphere through coagulation and gas-particle conversion (e.g.,
191 condensation and evaporation) processes. Airborne particles in the SOWC model influence
192 meteorological conditions through radiative feedbacks and microphysical processes. The
193 model simultaneously tracks particle mass, number concentration, and radius. The number
194 concentration and radius of different particle size bins from each source type are included as
195 the last two elements in the species dimension. Simulations in this study use 38 chemical
196 species (Table 1) from 5 emissions sources (wood smokes, gasoline, diesel, meat cooking,
197 and other aerosol types) and 8 size bins. The initial particle sizes from emissions are
198 0.005055, 0.1105, 0.221, 0.4415, 0.8835, 1.767, 3.535, and 7.0693 microns. Note that the
199 SOWC model uses moving size bins whose sizes change in response to gas-particle
200 conversion during model simulations. The model conserves aerosol mass concentration
201 throughout the simulation of atmospheric processes including emissions, transport,
202 deposition, coagulation, and condensation/evaporation. The gas-phase species emitted from

203 different sources in each grid cell are not tracked separately in the SOWC model at the
204 present time. In the current study, the initial and boundary conditions of aerosol particles are
205 based on observations from the California Regional Particulate Air Quality Study (CRPAQS)
206 (Ying et al., 2008). The distribution of particle emissions for different bins for every source
207 are calculated using emissions inventories provided by the California Air Resources Board
208 (CARB) along with measured chemical speciation profiles (Ying et al., 2008). Further
209 details of the SOWC model structure and source-oriented chemistry processes are described
210 by Zhang et al. (2014) and Joe et al. (2014).

211 **2.2 Cloud microphysics scheme**

212 The original Purdue Lin microphysics scheme was designed as a one-moment water
213 mass conserved microphysics scheme with five hydrometeors: cloud water, rain, cloud ice,
214 snow, and graupel (Lin et al., 1983; Chen and Sun, 2002). Chapman et al. (2009) added a
215 prognostic treatment of cloud droplet number (Ghan et al., 1997) to the Purdue Lin scheme to
216 make a two-moment treatment of cloud water within WRF/Chem. In our study, a source-
217 oriented CCN module was added to the SOWC model to track size-resolved information
218 about activated CCN from various aerosol sources. A new source-oriented 6D cloud
219 variable, “CLDAQC” (X, Z, Y, Size Bins, Source Types, Species) was added to SOWC to
220 describe source-oriented clouds. Droplet radius and number concentration are once again
221 stored as the last two elements in the species dimension of the CLDAQC variable. In the
222 Purdue Lin scheme, all microphysics processes are parameterized with water mass, except
223 autoconversion. ~~Chapman et al. (2009) added the autoconversion parameterization from Liu~~
224 ~~et al. (2005) into the Purdue Lin microphysics, which depends on cloud droplet number.~~
225 ~~Chapman et al. (2009)~~Chapman et al. (2009) added the autoconversion parameterization from
226 Liu et al. (2005) into the Purdue Lin microphysics, which depends on cloud droplet number.
227 Chapman et al. (2009) also specified changes to cloud droplet number proportional to the

228 microphysics process rate of cloud water mass. For example, when 10% cloud water
229 becomes rain water after autoconversion, 10% cloud droplets will be moved at the same time.

230 The continuity equation of the mass-coupled mixing ratio of CLDAQC can be written as
231 follows:

$$232 \quad \frac{\partial CLDAQC}{\partial t} = \nabla \cdot \vec{V} CLDAQC + \nabla \cdot K \nabla CLDAQC + P_{AACT} + S_{micro}, \quad (1)$$

233 where \vec{V} is the 3D wind vector and K is the eddy diffusion coefficient. The first two terms on
234 the right hand side of Eq. (1) are the flux divergence of CLDAQC (transport) and sub-grid
235 eddy mixing, respectively. Figure 1 shows the schematic diagram of the sinks and sources of
236 CLDAQC in the cloud microphysics processes (P_{AACT} and S_{micro}). Aerosol activation (P_{AACT})
237 is the main source of CLDAQC. The calculation of aerosol activation is based on a
238 maximum supersaturation determined from a Gaussian spectrum of updraft velocities and
239 aerosol chemistry composition for each size bin (Abdul-Razzak and Ghan, 2002). This
240 parameterization of aerosol activation was implemented in WRF/Chem model (Chapman et
241 al., 2009) and is used in this study. Aerosol activation was calculated each time step. Once
242 the environment reached the critical supersaturation, AQC activated as CCN. Water vapor
243 condenses at a diffusion limited rate to cloud droplets (water molecules transferred from
244 vapor to cloud in Purdue Lin scheme) and particle mass/number is transferred from the
245 interstitial aerosol variable (AQC) to the cloud-borne aerosol variable (CLDAQC). The
246 Purdue Lin microphysics scheme uses a saturation adjustment approach (i.e., it adjusts water
247 vapor to the saturation mixing ratio), so CCN activation is calculated before saturation
248 adjustment. After saturation adjustment, the condensation rate due to vapor diffusion is
249 proportional to particle size (Rogers and Yau, 1989). Results from CCN activation tests at
250 relevant supersaturation are discussed in Section 4.3.

251 Sinks and sources of CLDAQ (S_{micro}) are based on interactions between a cloud droplet
252 and the other hydrometeors (e.g., ice, rain, snow, and graupel) that can remove water from or
253 add water to CLDAQ. The sinks of cloud water, as well as CLDAQ, include
254 autoconversion from cloud to rain (P_{RAUT}) and the accretion of cloud water by rain (P_{RACW}),
255 snow (P_{SACW}), and graupel (P_{GACW}). The exchange between cloud water and cloud ice can
256 also occur through homogenous freezing of cloud water to ice (P_{IHOM}) and melting of cloud
257 ice to cloud water (P_{IMLT}). Finally, the condensation (associated with P_{ACCT}) and evaporation
258 of cloud water (P_{CEVP}) are implicitly taken into account in the Purdue Lin microphysics
259 scheme. When cloud droplets fully evaporate (sink of CLDAQ), the residual cores are
260 released back into the corresponding source type and size bin of the aerosol (AQC) variable.

261 **2.3 Radiation schemes**

262 The NASA Goddard shortwave and longwave radiation schemes (Chou and Suarez,
263 1999b, 2001b) are used in conjunction with the source-oriented cloud droplet algorithms in
264 the enhanced SOWC model. Absorption of radiation by water vapor, ozone, oxygen, carbon
265 dioxide, cloud droplets and aerosol particles is considered. Interactions among the absorption
266 and scattering by clouds and aerosols (Mie scattering), molecules (Rayleigh scattering) and
267 the surface are fully accounted for (Skamarock et al., 2008). Three main optical parameters
268 are calculated for each model layer to describe the influence of aerosols on the radiation:
269 aerosol optical thickness (τ), single scattering albedo (ω), and asymmetry factor (g). In the
270 present study, the numerical code described by Ying and Kleeman (2003) was implemented
271 to calculate the optical properties of source-oriented particles. The original numerical code
272 of Mie scattering developed by Bohren and Huffman (1983) was used to calculate the particle
273 extinction efficiency, scattering efficiency and asymmetry factor. The partial molar
274 refractive index approach described in Stelson (1990) was used to estimate the mean
275 refractive index for multi-component aerosols. .

276 For any wavelength of shortwave or longwave radiation (λ), the aerosol optical thickness
 277 (τ_a) of a model layer with depth h (m) containing a number concentration $n_a(r)$ ($\# \text{ m}^{-3} \mu\text{m}^{-1}$)
 278 of droplets with radius r (μm) is given by

$$279 \quad \tau_a(\lambda) = \pi h \int_0^\infty Q_e(\lambda, r) r^2 n_a(r) dr, \quad (2)$$

280 where, Q_e is the dimensionless extinction efficiency. The equivalent definition of aerosol
 281 optical thickness for discrete size bins j with a mean radius r_j (μm) can be written as

$$282 \quad \tau_a(\lambda) = \pi h \sum_i^n \sum_j^m Q_{e,i,j}(\lambda, r) r_{i,j}^2 N_{i,j}, \quad (3)$$

283 where subscript i refers to emission source, subscript j refers to size, n is the number of
 284 particle source types and m is the number of particle sizes. N ($\# \text{ m}^{-3}$) is the number of
 285 particles. The mean asymmetry factor (g_a) and single scattering albedo (ω_a) are calculated
 286 using the method described in (Yang, 2000):

$$287 \quad g_a(\lambda) = \frac{\sum_i^n \sum_j^m Q_{s,i,j}(\lambda, r) g_{i,j}(\lambda, r) N_{i,j} \pi r_{i,j}^2}{\sum_i^n \sum_j^m Q_{s,i,j}(\lambda, r) N_{i,j} \pi r_{i,j}^2}, \quad (4)$$

$$288 \quad \omega_a(\lambda) = \frac{\sum_i^n \sum_j^m Q_{s,i,j}(\lambda, r) N_{i,j} \pi r_{i,j}^2}{\sum_i^n \sum_j^m Q_{e,i,j}(\lambda, r) N_{i,j} \pi r_{i,j}^2}, \quad (5)$$

289 where Q_s is the dimensionless scattering efficiency. All of the optical parameters are
 290 functions of the wavelength (λ) of incident radiation.

291 In the original Goddard radiation schemes, cloud droplets are assigned to a mono-
 292 disperse size distribution (mean effective radius) which depends on the water mass and
 293 number concentration. The source-oriented cloud (CLDAQC) contains size distribution and
 294 chemistry information which is more realistic than the mono-disperse assumption. Equations

Field Code Changed

295 3-5 are applied to all size bins of not only the AQC but also the CLDAQC variables to
296 calculate optical properties and radiative forcing.

297 3. Numerical experiment designs

298 3.1 Fog event

299 A numerical simulation of fog was carried out with the SOWC model ~~as a convenient~~
300 ~~method~~ to test the effects of particle mixing state on warm clouds processes. Fog is an
301 excellent scientific case study that can isolate cloud activation and diffusive growth, the first
302 step of aerosol-cloud-radiation interactions, from other microphysical processes that usually
303 do not occur in fog, such as collision/coalescence, riming, melting, and aggregation. This
304 paper presents the development of the CLDAQC treatment within the SOWC model to
305 ensure that the model performs properly. A careful selection of a weather phenomenon is
306 important to evaluate the model performance and the impact of the aerosol mixture states on
307 cloud formation. The involvement of other hydrometeors, in addition to cloud droplets, can
308 not only change the cloud properties and cloud lifetime, but also modify the energy budget.
309 These extremely nonlinear processes can significantly complicate the evaluation of the model
310 performance and the first step of aerosol-cloud-radiation interaction. Thus we choose fog as
311 our very first weather system study for the evaluation of aerosol-cloud-radiation interactions
312 using the improved SOWC model. The influence of particle size and composition on fog
313 formation and droplet growth has been studied in previous field experiments (~~Frank et al.,~~
314 ~~1998; Moore et al., 2004; Ming and Russell, 2004; Cubison et al., 2008; Niu et al., 2012~~)(~~Frank~~
315 ~~et al., 1998; Moore et al., 2004; Ming and Russell, 2004; Cubison et al., 2008; Niu et al.,~~
316 ~~2012~~) and modeling studies (~~Bott and Carmichael, 1993; Kleeman et al., 1997~~)(~~Bott and~~
317 ~~Carmichael, 1993; Kleeman et al., 1997~~). ~~The results indicate that particle chemical~~
318 ~~composition and mixing state strongly influence fog droplet activation, mirroring the~~
319 ~~processes of interest for cloud droplets.~~

320 . The results indicate that particle chemical composition and mixing state strongly
321 influence fog droplet activation, mirroring the processes of interest for cloud droplets. For
322 example, the IPAC-NC field campaign in China observed clouds formed in a polluted
323 environment with RH below 100% due to high hygroscopic pollutants (Ma et al., 2010).

324 Tule fogs (radiation fog) frequently form in the Central Valley of California during the
325 winter season (Hayes et al., 1992). Winter in the Central Valley is associated with the
326 maximum concentration of airborne particulate matter (PM) (Chow et al., 1993) which is
327 composed of aerosol particles that can act as CCN. We chose ~~this challenging weather~~
328 ~~system for the first study of this kind since~~ Tule fog ~~as our case study since it~~ is important in
329 safety, hydrology and agriculture in California. ~~Fog is also an excellent scientific case study~~
330 ~~that can isolate cloud activation and diffusive growth, the first step of aerosol-cloud radiation~~
331 ~~interactions, from other microphysical processes which usually do not occur~~ aerosols in
332 ~~fog~~. California have been carefully investigated using the SOWC model (Joe et al., 2014;
333 Zhang et al., 2014). In the present study, a thick fog event that occurred on 16 and 17
334 January 2011 (Fig. 2) was chosen to investigate the impact of ~~source-oriented aging process-~~
335 ~~included~~ aerosol-cloud-radiation interactions on fog formation. Fog started forming over the
336 northern Central Valley on 13 January with observed surface relative humidity reaching 95-
337 100% and extended to the southern Central Valley on 14 January. The fog became thicker on
338 16 January and reached the maximum on 17 January (Fig. 2). This is evident by retrieved
339 cloud optical thickness from MODIS (discussed later). The fog started dissipating from the
340 northern Central Valley on 18 January and fully dissipated on 19 January (Fig. 2c).

341 In addition to calm wind and radiative cooling, high moisture is an important ingredient
342 to a Tule fog event in the Central Valley, California. Figure 3 shows the time series of
343 column integrated water vapor, sea level pressure, and 850-hPa wind vectors from ECMWF
344 Interim reanalysis data. On 11 January, the column water vapor (CWV) was very low, less

Formatted: Font color: Auto

345 than 10 mm, over the Central Valley (Fig. 3a). Moisture was advected into the Central
346 Valley (Fig. 3b) by a winter cyclone moving close to the northwestern coast of the United
347 States on 12 January. A weak southwest-northeast-oriented atmospheric river with a width of
348 1000 km and a maximum CWV of ~26-28 mm approached the western coast and brought
349 moisture into the Central Valley. At 0000 UTC 13 January (Fig 3c), moisture content began
350 increasing in the northern Central Valley. At night, drainage flow from the surrounding
351 mountains brought cold air into the Central Valley, mixed with the low-level moist air, and
352 initiated fog formation over the northern Central Valley. On 14 January (Fig. 3d), the CWV
353 over the southern Central Valley reached 22-24 mm and fog formed over the southern
354 Central Valley.

355 On 15 and 16 January, a more intense, west-southwest to east-northeast oriented
356 atmospheric river advected moisture into northern California (Figs. 3e and f). The moisture
357 in the Central Valley reached a maximum on 17 January (Fig. 3g), at the time when the fog
358 reached its maximum thickness during the study period (Fig. 2; also see the cloud optical
359 thickness discussion later). On 18 January (Fig. 3h), while high moisture and fog still
360 presented over the southern Central Valley, the moisture decreased and the fog disappeared
361 over the northern Central Valley. Fog fully dissipated in the Central Valley on 19 January.

362 According to the satellite images and surface temperature variation, the coverage and
363 thickness of fog followed a diurnal pattern with thinning in the daytime and thickening at
364 night. As mentioned earlier, the aerosol mixture state can impact fog formation and
365 properties of cloud droplets.

366 3.2 Observational data

367 Multiple types of measurement data were used to evaluate the SOWC model
368 performance. Moderate Resolution Imaging Spectroradiometer (MODIS) level 2 cloud
369 products from the Terra and Aqua satellites provide 5-km resolution cloud optical thickness

370 (COT) and liquid water path (LWP). The LWP retrieval from MODIS has been used to study
371 low cloud and fog (Bendix et al., 2005). High-resolution MODIS data can describe fog
372 spatial distribution and intensity but are only available once every 24 hours (daytime only)
373 from each satellite. The SOWC model predictions for temperature and moisture at the
374 surface are also evaluated against *in situ* time-series meteorological data from 24 surface
375 weather stations along with net ground shortwave fluxes at 42 sites from California Irrigation
376 Management Information System (CIMIS). Measured concentrations of airborne particles
377 were obtained from the California Ambient Air Quality Data (CAAQD) provided by the
378 Planning & Technical Support Division (PTSD) of the California Air Resources Board
379 (CARB). The station details of CAAQD are provided in Table 2. The locations of all
380 measurement sites are provided in Fig. 4.

381 3.3 Numerical experiment design

382 The primary objective of this study is to examine how the source-oriented (S_) (*i.e.*,
383 [aging-process-included](#)) and internal (I_) mixture representations of aerosol particles differ in
384 their feedbacks to meteorology in a fog event. Internally mixed simulations (I_) artificially
385 blend emissions from all sources into a single particle size distribution thereby concealing all
386 advanced treatments of particle mixing and aging. Four experiments were carried out (Table
387 3) for the selected fog event. In the basecase experiment of S_ARon_CRmod, the polluted
388 aerosol particles tracked by AQC act as the source of CCN (S_) and the aerosol-radiation
389 interaction (aerosol direct effect) is enabled in the radiation schemes (ARon). The geometric-
390 optics approach mentioned in Section 2.3 is used to calculate the cloud optical properties of
391 each model layer (CRmod). S_ARon_CRorig is similar to S_ARon_CRmod, except for the
392 use of the original cloud optical property calculation (CRorig) in the NASA Goddard
393 shortwave and longwave radiation schemes. As discussed previously, the original schemes
394 are based on an estimate of the cloud droplet effective radius using the cloud mass and

395 number concentration (CRorig). The radius of cloud droplets in the original Goddard
396 shortwave radiation scheme is constrained to the range from 4 μm to 20 μm . In the modified
397 cloud-radiation scheme (CRmod), the size range of cloud droplets in Eq. (3) can vary
398 between ~~the dry aerosol particle radius~~ activated CCNs to 30 μm . S_ARoff_CRmod has no
399 aerosol direct effect in the radiation schemes (ARoff). The comparison of S_ARoff_CRmod
400 and S_ARon_CRmod is used to estimate the aerosol direct effect in this study.

401 Each numerical experiment employed two domains with two-way nesting. Domain 1
402 (86 x 97 grid cells) had a resolution of 12 km while domain 2 (127 x 202 grid cells) had a
403 resolution of 4 km. Domain 2 was positioned to cover the entire Central Valley of California
404 and results from this domain are used for the subsequent analysis. All simulations used 31
405 vertically staggered layers based on a terrain-following pressure coordinate system. The
406 vertical layers are stretched with a higher resolution near the surface (an average depth of ~30
407 m in the first model half layer). Variables other than vertical velocity and geopotential were
408 stored in the half model levels. The time step was 60 seconds for the first domain and 20
409 seconds for the second domain. The physics schemes employed for the simulations included
410 the modified Purdue Lin microphysics scheme (Chen and Sun, 2002), the NASA Goddard
411 longwave/shortwave radiation schemes (Chou and Suarez, 1999a, 2001a), the Kain-Fritsch
412 cumulus scheme (Kain and Fritsch, 1990; Kain, 1993) (domain 1 only), the YSU PBL
413 scheme (Hong et al., 2006; Hong, 2010) and the Noah LSM surface scheme (Tewari et al.,
414 2007). No cumulus scheme is used in the inner-most domain (4 km resolution). The number
415 of cloud droplets was not considered in the convective scheme in the SOWC model. The
416 target episode had calm winds with local fog formation in the Central Valley (not
417 propagating in through lateral boundaries). Moreover, the event occurred in the winter
418 season when the Convective Available Potential Energy (CAPE) was small. Therefore, the
419 KF cumulus convective parameterization is inactive for this cases study. The meteorological

420 initial and boundary conditions were taken from North American Regional Reanalysis
421 (NARR), which has a spatial resolution of 32 km and a temporal resolution of 3 hours.

422 The SOWC model tracked two 6D variables for aerosol/cloud properties which
423 introduce considerable computational burden for model simulations when compared to
424 standard WRF/Chem model simulation (with prescribed aerosol concentration). The
425 computational cost of the SOWC model, which is proportional to the extra information that is
426 tracked, is approximately 25 times greater than the standard WRF/Chem 3.1.1 simulation
427 with prescribed aerosols (chem_opt = 0) or approximately 5 times greater than the standard
428 WF/Chem 3.1.1 simulation with any chemistry option (/=0) in the current study. SOWC
429 model simulations started at 0000 UTC 9 January (7 days prior to the start of the thick fog
430 event) with four-dimensional data assimilation (FDDA), which nudges model fields in
431 domain 1 to analysis including the u and v components of horizontal winds, water vapor
432 mixing ratio, and temperature above the PBL height in all simulations. This approach
433 provides a realistic heterogeneous aerosol distribution and low-level temperature and
434 moisture fields at the start of the thick fog simulation. Observations from surface stations
435 and NARR data were used for nudging during this aerosol spin-up period. Between 0000
436 UTC 16 January to 0000 UTC 19 January, the SOWC model integrated without FDDA (3
437 day free run) during which time the effects of the different model configurations were
438 observed and is our major interested time period.

439 **4. Model Results**

440 **4.1 Evaluation of basecase (S_ARon_CRmod) model performance**

441 The SOWC model calculates CCN number concentrations based on the activation of
442 aerosols (AQC). The AQC number concentration can influence the intensity of initial fog
443 formation and spatial distribution of final fog fields, and thus AQC number concentration is

444 examined first. Figure 5 shows 72-hour averaged (from 16 to 18 January 2011) AQC number
445 concentrations in California's Central Valley that were also averaged over the first five model
446 layers for S_ARon_CRmod. Fog usually forms within the planet boundary layer (PBL),
447 which reaches to a height of approximately five model layers in winter conditions in the
448 Central Valley (450-550 m). Temporally averaged AQC concentrations are approximately
449 $2 \times 10^9 \text{ \# m}^{-3}$, with the highest concentrations predicted in the vicinity of polluted cities (e.g.,
450 the San Francisco Bay Area, Stockton, Modesto, Sacramento, Fresno, and Bakersfield), in the
451 middle of the Central Valley, and at foothills of Sierra Nevada Mountain over the east-
452 southeastern Central Valley.

453 Figure 6 shows the comparison of simulated nitrate (NO_3^-), sulfate (SO_4^{2-}), ammonium
454 (NH_4^+) and soluble sodium (Na^+) concentrations to measured values at 6 monitoring stations
455 (see Table 2 and Fig. 4) on 18 January 2011. Simulated sulfate and soluble sodium are in
456 reasonable (>80%) agreement with measurements but nitrate and ammonium concentrations
457 were under predicted by approximately 70%. The cause for this discrepancy is unknown, but
458 one possibility is the presence of organic nitrate compounds in the atmosphere that are not
459 simulated by the model chemistry. Note that both observed and predicted nitrate
460 concentrations in the current episode are lower than the maximum concentrations observed in
461 historical extreme episodes within the San Joaquin Valley (SJV) because the current
462 stagnation event only lasted a few days while extreme events last multiple weeks. If more
463 discussion of aerosol perditions form the SOWC model is desired, we refer the reader to
464 Zhang et al. (2014) who present a comparison of predicted aerosol concentrations and
465 measured concentrations using field campaign data measured during the California Regional
466 PM_{10} / $\text{PM}_{2.5}$ Air Quality Study (CRPAQS) in December 2000 – January 2001.

467 The S_ARon_CRmod experiment reasonably reproduces the observed spatial
468 distribution and magnitude of liquid water path (LWP) compared to the data retrieved from

469 MODIS (Fig. 7). In particular, the model predicts LWP well over the northern portion of the
470 Central Valley during the fog event (16 to 18 January). However, the model under-predicts
471 LWP in the middle portion of the Central Valley, which caused the fog to dissipate earlier
472 (late 17 January). Once the surface temperature increases in one area due to thin fog, the
473 dissipation spreads out quickly until the fog completely evaporates. For the southern portion
474 of the Central Valley, the fog event starts earlier (14 to 15 January) and the model reasonably
475 predicts the onset of the event. But the simulated fog is too dense (figure not shown). In
476 addition, the peak of the simulated fog occurs one day earlier (16 January forecast versus 17
477 January observed). This timing difference could be caused by the change in the microphysics
478 processes at 0000 UTC 16 January. During the FDDA time period (before 16 January), the
479 one-moment bulk microphysics scheme is used. After the FDDA time period, aerosols start
480 being involved in cloud formation. High Nitrate concentrates in the SJV and enhances
481 aerosol activation due to its high hygroscopicity. This could partially explain why the peak
482 of the LWP occurs on 16 January. The details of aerosol chemical properties are discussed
483 by Zhang et al. (2014).

484 While simulated LWP is comparable to MODIS retrievals with one-day shift (Fig. 7),
485 ~~high to obtain a higher COT than observed (Fig. 8b versus 8c) we expect that the model~~
486 ~~produces more small cloud droplets with a higher CCN concentration and smaller cloud~~
487 ~~droplets, thus high COTs (Fig. 8), are predicted in the SOWC simulations, especially in over~~
488 highly polluted areas. High predicted COT results in cold surface temperature, especially in
489 the southern portion of the Central Valley. Overall, the spatial distribution and magnitude of
490 simulated COT also match the satellite data reasonably (Fig. 8), except for the overestimation
491 of COT over the southeastern Central Valley (Fig. 8b and d).

492 Mean biases of 2-m temperature (T2), 2-m water vapor mixing ratio (Q2), and surface
493 net downward shortwave radiative flux (NSF) over the entire Central Valley from 16 to 18

Formatted: Font color: Text 1

Formatted: Font color: Text 1

Formatted: Font color: Text 1

Formatted: Font color: Text 1

Formatted: Font color: Text 1

494 January 2011 for S_ARon_CRmod are calculated (Fig. 9). Generally, T2 and Q2 of
495 S_ARon_CRmod are under-predicted by 2 °C and 0.7 g kg⁻¹, respectively. The predicted
496 time variation of T2 and Q2 biases is small in the first one and half days but increases after
497 1600 UTC 17 January because the predicted fog dissipated in the daytime, different from
498 observations. Since the predicted fog dissipated, simulated NSF increased and was over-
499 predicted by 13.9 W m⁻². Low simulated T2 and Q2, particularly during first one and half
500 days, in S_ARon_CRmod are partially due to over-predictions of the fog formation (i.e., too
501 much condensation leading to depleted water vapor), especially over the southern portion of
502 the Central Valley. Overall, S_ARon_CRmod reasonably forecasted LWP and COT spatial
503 pattern and intensity. S_ARon_CRmod also captured the diurnal pattern of T2 and Q2 during
504 the fog event, but under-predicted the absolute magnitude of T2 and Q2 by 1.76 (2.22) °C
505 and 0.56 (0.88) g kg⁻¹ in the daytime (nighttime), respectively.

506 **4.2 Source-oriented aerosol direct and indirect effects**

507 S_ARoff_CRmod is designed to test aerosol-radiation feedback and so the comparison
508 between S_ARoff_CRmod and S_ARon_CRmod can help quantify the aerosol direct effect
509 in the current study. Table 4 shows that the hourly bias mean and standard deviation from 24
510 surface stations in the daytime and nighttime of S_ARoff_CRmod are similar to, but larger
511 than, results from S_ARon_CRmod for T2 and Q2 at the ground. However, compared to
512 S_ARon_CRmod, the smaller cold bias from S_ARoff_CRmod is consistent with its larger
513 net downward shortwave radiative flux (NSF) shown in Tables 4 and 5. Table 5 shows that
514 the average NSF within the entire Central Valley from S_ARoff_CRmod is higher than
515 S_ARon_CRmod by 3.7 W m⁻², which means that the shortwave energy flux that reached the
516 ground was reduced by ~3.7 W m⁻² due to aerosol radiative forcing in this case study. The
517 maximum increases of T2 and NSF by the aerosol direct effect occurred on 17 January 2011
518 (Fig. 9). Table 5 also shows the mean value of cloud liquid water-mixing-ratio, cloud droplet

519 number, surface skin temperature, latent heat flux and sensible heat flux over the Central
520 Valley during 16 to 18 January 2011. Cloud ~~liquid water-mixing-ratio~~ and cloud droplet
521 number were averaged within the first five model layers. The aerosol direct effect leads to
522 increases in the cloud water mass and cloud droplet number by 3.3% and 4.5%, respectively,
523 due to reductions in skin temperature (0.1 K) and net shortwave flux (3.7 W m⁻²).

524 The modified radiation schemes for cloud optical properties in the S_ARon_CRmod
525 experiment do not have significant feedback on spatially and temporally averaged cloud
526 water mass ~~and cloud droplet number~~ (i.e., compared to S_ARon_CRorig) as shown in Table
527 5. ~~Theoretically~~However, the modified cloud-radiation interaction (i.e., geometric-optics
528 method) used in the COT calculations (S_ARon_CRmod) ~~can predict~~predicts slightly higher
529 COT, which leads to slightly lower net shortwave flux and surface skin temperature,
530 especially in the polluted area. The higher COT predictions are likely caused by differences
531 in the size range of cloud droplets and refractive indexes of cloud water with/without
532 chemical composition in the calculation of cloud radiative properties. ~~As mentioned above,~~
533 ~~the~~In the original radiation scheme, the cloud optical thickness (COT) is a function of cloud
534 ~~water path (CWP) and an effective~~ radius ($4 \mu\text{m} \leq r_e \leq 20 \mu\text{m}$), which is derived from the
535 ~~water mass and the total droplet number assuming a uniform size~~ of cloud droplets ~~in the~~
536 ~~original Goddard shortwave radiation scheme is constrained to the range from 4 μm to 20~~
537 ~~μm, while in our:~~

$$\tau_{orig}(\lambda) = CWP \times \left(-6.59 \times 10^{-3} + \frac{1.65}{r_e}\right) \quad (6)$$

539 ~~In the~~ modified radiation scheme, ~~the cloud droplets~~ in S_ARon_CRmod, the COT is
540 ~~calculated based on simulated cloud droplet size, number, and chemical composition of each~~
541 ~~bin and source (Eq. 3). In addition, the formula of COT, single scattering albedo and~~
542 ~~asymmetry factor in the modified radiation scheme~~ are ~~allowed to range~~all modified. With a
543 ~~similar Q_e, although Q_n in size~~S_ARon_CRorig is higher than that in S_ARon_CRmod, the

Formatted: Font color: Text 1

544 COT is slightly higher in S_ARon_CRmod due to different formulas used in the calculation
545 of cloud-radiation interaction. The small difference of COT between the dry aerosol particle
546 radius to 30 μm . The these two experiments in fact indicates that the parameterization of
547 cloud optical thickness COT in the original Goddard radiation scheme assumes that cloud
548 droplets are pure water. The modified radiation scheme recognizes the chemical species in
549 the cloud water and considers these species when calculating the cloud droplet index of
550 refraction. However, in this case study the results of these two experiments (i.e.,
551 S_ARon_CRmod and S_ARon_CRorig) were very similar. provides a reasonable result
552 compared to the explicit COT calculation.

553 Because the meteorological conditions of the fog event are calm and stable, the cloud
554 microphysics processes are fairly slow and simple (no rain produced in this case). Although
555 S_ARon_CRorig had slightly higher cloud droplet number concentrations, the modified
556 calculation of the cloud optical properties in S_ARon_CRmod gave a similar cloud amount
557 and net shortwave radiation flux reaching the surface, which produced nearly identical
558 feedbacks to meteorology in both experiments (Table 5).

559 **4.3 Internal mixture versus source-oriented aerosols**

560 The mixing state of chemical components among the atmospheric aerosol particles can
561 potentially play an important role in fog formation. The activation of aerosol particles into
562 cloud droplets depends on the critical ~~super saturation~~ supersaturation which in turn depends
563 on particle composition. According to the Köhler equation, increased concentrations of
564 solutes will decrease the critical ~~super saturation~~ supersaturation required to activate a particle
565 into a CCN. As mentioned earlier, hydrophobic particles (i.e. black carbon) will more easily
566 serve as CCN once they are coated with hygroscopic material (i.e. sulfate). Increased
567 concentrations of solutes can potentially modify the frequency and severity of fog events in
568 polluted air. In this section, we compare results from S_ARon_CRmod (source-oriented (i.e.,

569 [aging-process-included](#)) experiment) and I_ARon_CRmod (internally mixed experiment) to
570 investigate the activation change and further meteorological responses between internally
571 mixed and source-oriented aerosols. The internally mixed experiment is conducted by
572 lumping all sources together (i.e., AQC source dimension collapsed to one producing a 5D
573 AQC variable).

574 It is likely that the ratio of CCN concentration (N_{CCN}) to total aerosol concentration
575 (N_{CN}) will be different for each of the five source types tracked in S_ARon_CRmod since the
576 CCN activation depends on the chemical composition and size of the particles. The highest
577 ratio of N_{CCN}/N_{CN} for S_ARon_CRmod and I_ARon_CRmod is located in the southern
578 Central Valley (Fig. 10) due to higher moisture from the atmospheric river resulting in
579 greater aerosols activation to CCNs and smaller residual aerosol number concentration (see
580 Fig. 5). Over the Central Valley during 16 to 18 January 2011, the ratio of N_{CCN}/N_{CN} for
581 each source type is 12.63%, 15.60%, 14.89%, 16.80% and 20.21% for wood smoke, gasoline,
582 diesel, meat cooking, and others, respectively (averaged within the first five model layers).
583 Wood smoke is typically a major source of aerosol (~38%) in California's Central Valley
584 during winter stagnation events (see Table 6) and the organic carbon in wood smoke is water-
585 soluble (Dusek et al., 2011) which allows these particles to activate more easily than
586 insoluble particles. However, the majority of the wood smoke particles are located in the
587 smallest size bin, so the ratio of N_{CCN}/N_{CN} for wood smoke is comparable with that of
588 hydrophobic diesel. The source type of "others", which has the highest ratio of N_{CCN}/N_{CN} , is
589 dominated by larger dust particles coated with secondary components such as nitrate and are
590 easier to activate, in contrast to the smaller combustion particles emitted from other tracked
591 sources.

592 The comparison of the average ratio of N_{CCN}/N_{CN} from the first five model layers
593 between S_ARon_CRmod and I_ARon_CRmod is shown on Fig. 10. The spatial patterns

594 produced by both experiments are similar but I_ARon_CRmod has a higher N_{CCN}/N_{CN} ratio,
595 in particular over the northern two thirds of the Central Valley. The largest differences
596 between N_{CCN}/N_{CN} predicted by S_ARon_CRmod and I_ARon_CRmod occur in regions
597 with large emissions of wood smoke (figure not shown). The ratio of N_{CCN}/N_{CN} for both
598 experiments can reach >30% but the highest N_{CCN}/N_{CN} ratio occurs in relatively less polluted
599 regions. The spatially averaged ratio of N_{CCN}/N_{CN} is 16.65% for S_ARon_CRmod and
600 27.49% for I_ARon_CRmod within the Central Valley over the period of 16 to 18 January.
601 The CCN concentrations and N_{CCN}/N_{CN} ratios between internally mixed and source-oriented
602 experiments at different ~~super-saturations~~supersaturations were calculated to better
603 understand this result. Figure 11a shows the 72-hour averaged CCN concentration at ~~super-~~
604 ~~saturations~~supersaturations of 0.02%, 0.05%, 0.1%, 0.2% and 0.5% and total AQC
605 concentration averaged within the first five model layers. Figure 11b presents corresponding
606 N_{CCN}/N_{CN} ratios at 5 different ~~super-saturations~~supersaturations. When the ~~super-~~
607 ~~saturations~~supersaturation is less than or equal to 0.2%, the N_{CCN}/N_{CN} ratio predicted from
608 S_ARon_CRmod is comparable or even slightly higher than that predicted from
609 I_ARon_CRmod. In the S_ARon_CRmod tests, 56% of the particles tracked in the AQC
610 variable (mainly in size bins 2-8) are activated as CCN. When the ~~super-~~
611 ~~saturations~~supersaturation is close to 0.5%, the N_{CCN}/N_{CN} ratio from I_ARon_CRmod can be
612 15% higher than that of S_ARon_CRmod. Most particles tracked in the AQC size bin 1 can
613 activate in the internally mixed experiment; however, in the source-oriented experiment only
614 particles in AQC size bin 1 associated with wood smoke and “others” sources activate due to
615 the relatively hydrophobic nature of particles associated with other sources (Table 6).
616 Cubison et al. (2008) emitted in AQC size bin 1 from wood smoke and “others sources” are
617 sufficiently hygroscopic to activate. The remaining sources are dominated by hydrophobic
618 compounds (such as elemental carbon) that do not activate under the study conditions (Table

Formatted: Font color: Text 1

Formatted: Font color: Text 1

619 [6. Cubison et al. \(2008\)](#) analyzed observational CCN and CN data in 2005 from a field
620 campaign in California and found that the average ratio of N_{CCN}/N_{CN} was 18% for a ~~super-~~
621 ~~saturation~~supersaturation value of 0.5%, but their predicted N_{CCN}/N_{CN} ratio based on the
622 internal mixture assumptions could reach to more than 50%. In the source-oriented SOWC
623 model, ~~super-saturation~~supersaturation values are typically ~0.2-0.3% with maximum value
624 of 0.5% in some areas. The estimated ratio of N_{CCN}/N_{CN} in the source-oriented model is
625 comparable with observations in Cubison et al. (2008), especially in polluted areas. The
626 temporal variations of mean bias of 2-m temperature (T2), 2-m water vapor mixing ratio
627 (Q2), and surface net downward shortwave radiative flux (NSF) between internal versus
628 external aerosol mixture states (I_ARon_CRmod versus S_ARon_CRmod) are similar
629 ~~until~~ 2000 UTC 17 January. After late 17 January, the bias differences between two
630 experiments are more apparent in the daytime than in the nighttime ([Fig. 9 and Table 4](#)).
631 Compared to I_ARon_CRmod, S_ARon_CRmod reduced bias in T2 by 0.25 K in the
632 daytime but had higher bias in NSF. S_ARon_CRmod did predict improved values of Q2.
633 Based on [Fig. 9](#), we know that the source-oriented and internal aerosol mixing states mainly
634 cause differences in surface temperature in the daytime. [Figures 12a and b](#) illustrate the
635 relative change $((\text{internally mixed} - \text{source-oriented})/\text{source-oriented} * 100\%)$ of averaged
636 (16 - 18 January 2011) cloud liquid water-~~mixing-ratio~~ and cloud droplet number,
637 respectively, during the daytime. I_ARon_CRmod predicts cloud liquid water-~~mixing-ratios~~
638 that are 40% higher than values predicted by S_ARon_CRmod over the northern Central
639 Valley ([Fig. 12a](#)). The largest relative change in predicted cloud water concentration also
640 occurs in the northern Central Valley near the mountains where fogs are initiated by drainage
641 flow. I_ARon_CRmod predicts higher cloud droplet number ([Fig. 12b](#)), with the largest
642 relative increases ~~(50-60%)~~ once again observed in areas near mountains and highly
643 polluted regions with more modest changes of 20~30% over remote regions. Internally

644 mixed aerosols reduce the critical saturation ratio for particles by artificially mixing
645 hygroscopic and hydrophobic components that in turn allows particles to activate more
646 easily.

647 The internally mixed experiment (I_ARon_CRmod) predicts lower daytime averaged
648 surface skin temperature and net downward shortwave flux at ground (Fig. 12c and d)
649 corresponding to the areas with higher cloud liquid water ~~mixing ratio~~ and cloud droplet
650 concentrations (Fig. 12a and b). This result is expected since higher cloud liquid water
651 ~~mixing ratio~~ and cloud droplet concentration will reduce the solar radiation flux on the
652 surface. The reduction of surface skin temperature in the internal mixed experiment is
653 proportional to the change of the net shortwave radiation. Figure 13 shows that the area
654 average of latent heat flux (LH) and sensible heat flux (SH) over the Central Valley in
655 S_ARon_CRmod and the average difference of internally mixed and source-oriented
656 experiments. Higher cloud amount and lower surface temperature are predicted in the
657 internally mixed experiment leading to reduced LH and SH fluxes at ground level compared
658 to the source-oriented experiment. The difference between internally mixed and source-
659 oriented predictions for LH and SH reached 3 W m^{-2} and 5 W m^{-2} , respectively, at noon local
660 time (2200 UTC 17 January).

661 Table 7 shows hourly mean bias and root-mean-square-difference between internally
662 mixed (I_ARon_CRmod) and source-oriented (S_ARon_CRmod) experiments for six
663 variables within the Central Valley during 16 to 18 January 2011. The mean bias between
664 these two experiments is $1.19 \times 10^{-2} \text{ (g m}^{-3}\text{)}$ for cloud liquid water ~~mixing ratio~~ and 6.24×10^7
665 $\text{(} \# \text{ m}^{-3}\text{)}$ for cloud droplet number. The direction of these trends is expected since internally
666 mixed aerosols are easier to activate as CCN. The mean bias between internally mixed and
667 source-oriented experiments is -0.15 (K) for surface skin temperature and $-6.02 \text{ (W m}^{-2}\text{)}$ for
668 net shortwave flux. The mean bias of LH and SH is -0.61 and $-0.36 \text{ (W m}^{-2}\text{)}$, respectively.

669 The root-mean-square-difference between these two experiments is large for each variable,
670 meaning that the difference varies strongly with location (see Fig. 12).

671 In summary, compared to S_ARon_CRmod, I_ARon_CRmod has a higher CCN / cloud
672 droplet number concentration because internally mixed aerosols can instantaneously contain
673 hygroscopic material (e.g. sulfate) through artificial mixing, which decreases the critical
674 supersaturation requirement for a particle to activate into a CCN, leading to higher cloud
675 number concentration and optical thickness. Thicker fog in I_ARon_CRmod reduces the
676 amount of shortwave radiation reaching the surface, resulting in a lower surface temperature.
677 A lower surface temperature can have a positive feedback on cloud lifetime (i.e., a longer
678 cloud lifetime), which further reduces shortwave radiation reaching the surface when
679 compared to S_ARon_CRmod. Hence, the aerosols that include aging processes can delay
680 CCN activation and produce fewer cloud droplets and less fog, which in turn will modify the
681 energy budget near the surface.

682 **5. Summary and discussion**

683 A warm cloud-aerosol interaction module was implemented into the source-oriented
684 Weather Research and Forecasting model with Chemistry (SOWC) to study the aerosol-
685 cloud-radiation interactions during fog simulations. The source-oriented mixture of aerosols
686 is used to explicitly simulate particle aging processes in the atmosphere rather than
687 instantaneously combining particles into an internal mixture. The SOWC model was used to
688 simulate a fog event in California's Central Valley in January 2011 with seven days of FDDA
689 nudging and three days of free run. Fog formation occurred when high moisture content
690 from an Atmospheric River was advected into the Central Valley and cold drainage flows
691 occurred into the valley at night. The initial tests used 5 emissions sources (wood smoke,
692 gasoline, diesel, meat cooking, and others) with particles from each source consisting of 38

693 chemical species and 8 size bins, spanning a diameter range from 0.01 to 10 microns. The
694 highest model spatial resolution was 4 km.

695 Four numerical experiments were conducted to test model performance, meteorological
696 feedbacks from internal and source-oriented aerosols, and the impact of aerosol-cloud-
697 radiation interaction on fog formation. Compared to observations, the SOWC model
698 reasonably predicted fog spatial distribution and duration and environmental meteorological
699 feedbacks. However, the model over-predicted liquid water path and cloud optical thickness,
700 which resulted in cold surface temperature bias. The inclusion of aerosol-radiation
701 interaction reduced net downward shortwave radiative flux by an average of 3.7 W m^{-2} and
702 daytime surface temperature by 0.1 K. Results that used different treatments for aerosol
703 mixing states were compared, and the important [findings/results](#) are: 1) the fraction of
704 N_{CCN}/N_{CN} at a supersaturation of 0.5% in the Central Valley decreased from 94% in the
705 internal mixture model to 80% in the source-oriented mixture model; 2) due to a smaller
706 number of the CCN concentration in the source-oriented mixture model than in the internal
707 mixture model, cloud [liquid water-mixing-ratio](#) and cloud droplet number decreased 5% and
708 15%, respectively; and 3) compared to observations, the source-oriented mixture model
709 reduced the cold bias for surface temperature by 0.25 K in the daytime relative to the internal
710 mixture model. The source-oriented mixture representation of particles also provided more
711 reasonable predictions for cloud droplet number and cloud water mass versus observations
712 due to different activation properties than the internal mixture representation of particles.
713 The internal mixture model predicted greater activation of CCN than the source-oriented
714 model due to artificial coating of hydrophobic particles with hygroscopic components.

715 The SOWC model in this study explicitly calculates primary particle aging over a
716 regional scale for fog formation prediction with two-moment microphysics scheme and
717 aerosol-cloud-radiation interactions. The SOWC model should be a useful tool to study

718 aerosol-cloud-radiation interactions. ~~We are now conducting more numerical studies on~~
719 ~~different weather systems to explore the full range of responses~~Note that the current
720 ~~results are based on a Tule fog case study in the Central Valley of California. Additional fog~~
721 ~~case studies under different weather conditions in other regions of the world are required to~~
722 ~~draw conclusions at those locations.~~

Formatted: Font: Times New Roman

Formatted: Font: Times New Roman, Font color: Auto

724 Acknowledgment

725 ~~The authors thank two anonymous reviewers for their insightful comments on the manuscript.~~

726 The authors would ~~also~~ like to ~~acknowledgethank~~ the WRF and WRF-Chem teams for their
727 efforts on model development. This study was funded by the United States Environmental
728 Protection Agency under Grant No. R833372, NASA Grant No. NNX09AC38G, and NASA
729 High-End Computing (HEC) Program through the NASA Advanced Supercomputing (NAS)
730 Division at Ames Research Center (SMD-13-3895). Although the research described in the
731 article has been funded by the United States Environmental Protection Agency it has not been
732 subject to the Agency's required peer and policy review and therefore does not necessarily
733 reflect the reviews of the Agency and no official endorsement should be inferred.

734 References

736 ~~Abdul-Razzak, H., and Ghan, S. J.: A parameterization of aerosol activation 3. Sectional~~
737 ~~representation, Journal of Geophysical Research: Atmospheres, 107, AAC 1-1-AAC 1-6,~~
738 ~~10.1029/2001jd000483, 2002.~~
739 Ackerman, A. S., Toon, O. B., Stevens, D. E., Heymsfield, A. J., Ramanathan, V., and Welton,
740 E. J.: Reduction of Tropical Cloudiness by Soot, Science, 288, 1042-1047,
741 10.1126/science.288.5468.1042, 2000.
742 Ackermann, I. J., Hass, H., Memmesheimer, M., Ebel, A., Binkowski, F. S., and Shankar, U.:
743 Modal aerosol dynamics model for Europe: development and first applications,
744 Atmospheric Environment, 32, 2981-2999, [http://dx.doi.org/10.1016/S1352-](http://dx.doi.org/10.1016/S1352-2310(98)00006-5)
745 [2310\(98\)00006-5](http://dx.doi.org/10.1016/S1352-2310(98)00006-5), 1998.
746 Adams, P. J., Seinfeld, J. H., Koch, D., Mickley, L., and Jacob, D.: General circulation model
747 assessment of direct radiative forcing by the sulfate-nitrate-ammonium-water inorganic
748 aerosol system, Journal of Geophysical Research-Atmospheres, 106, 1097-1111,
749 10.1029/2000jd900512, 2001.

Formatted: English (United States)

Formatted: EndNote Bibliography, Left

Formatted: Font: +Body (Cambria)

Formatted: English (United States)

750 Albrecht, B. A.: AEROSOLS, CLOUD MICROPHYSICS, AND FRACTIONAL CLOUDINESS,
751 Science, 245, 1227-1230, 10.1126/science.245.4923.1227, 1989.

752 [Anttila, T.: Sensitivity of cloud droplet formation to the numerical treatment of the
753 particle mixing state. Journal of Geophysical Research: Atmospheres, 115, n/a-n/a,
754 10.1029/2010JD013995, 2010.](#)

755 Bendix, J., Thies, B., Cermak, J., and Nauß, T.: Ground fog detection from space based on
756 MODIS daytime data—a feasibility study, Weather and forecasting, 20, 989-1005, 2005.

757 Binkowski, F. S., and Shankar, U.: The Regional Particulate Matter Model: 1. Model
758 description and preliminary results, Journal of Geophysical Research: Atmospheres,
759 100, 26191-26209, 10.1029/95jd02093, 1995.

760 Bohren, C. F., and Huffman, D. R.: Absorption and Scattering of Light by Small Particles,
761 Wiley, New York, 1983.

762 Bott, A., and Carmichael, G. R.: Multiphase chemistry in a microphysical radiation fog
763 model—A numerical study, Atmospheric Environment. Part A. General Topics, 27, 503-
764 522, [http://dx.doi.org/10.1016/0960-1686\(93\)90208-G](http://dx.doi.org/10.1016/0960-1686(93)90208-G), 1993.

765 Chapman, E. G., Gustafson Jr, W. I., Easter, R. C., Barnard, J. C., Ghan, S. J., Pekour, M. S.,
766 and Fast, J. D.: Coupling aerosol-cloud-radiative processes in the WRF-Chem model:
767 Investigating the radiative impact of elevated point sources, Atmos. Chem. Phys., 9, 945-
768 964, 10.5194/acp-9-945-2009, 2009.

769 Chen, J.-P., and Lamb, D.: Simulation of Cloud Microphysical and Chemical Processes
770 Using a Multicomponent Framework. Part I: Description of the Microphysical Model,
771 Journal of the Atmospheric Sciences, 51, 2613-2630, 1994.

772 Chen, J.-P., Hazra, A., Shiu, C.-J., Tsai, I.-C., and Lee, H.-H.: Interaction between Aerosols
773 and Clouds: Current Understanding, in: Recent Progress in Atmospheric Sciences:
774 Applications to the Asia-Pacific Region, edited by: Liou, K. N., and Chou, M.-D., World
775 Scientific Publishing Co. Pte. Ltd., 231-281, 2008.

776 Chen, S.-H., and Sun, W. Y.: A one-dimensional time-dependent cloud model, j. Meteor.
777 Soc. Japan, 80, 99-118, 2002.

778 Chou, M.-D., and Suarez, M. J.: A Solar Radiation Parameterization for Atmospheric
779 Studies NASA Tech. Rep. NASA/TM-1999-10460, 15, 1999a.

780 Chou, M.-D., and Suarez, M. J.: A Thermal Infrared Radiation Parameterization for
781 Atmospheric Studies, NASA Tech. Rep. NASA/TM-2001-104606, 19, 2001a.

782 Chou, M. D., and Suarez, M. J.: A solar radiation parameterization for atmospheric
783 studies., NASA Tech. Rep., 38, 1999b.

784 Chou, M. D., and Suarez, M. J.: A thermal infrared radiation parameterization for
785 atmospheric studies. , NASA Tech. Rep., 55, 2001b.

786 Chow, J. C., Watson, J. G., Lowenthal, D. H., Solomon, P. A., Magliano, K. L., Ziman, S. D.,
787 and Richards, L. W.: PM10 and PM2.5 Compositions in California's San Joaquin Valley,
788 Aerosol Science and Technology, 18, 105-128, 10.1080/02786829308959588, 1993.

789 Cubison, M. J., Ervens, B., Feingold, G., Docherty, K. S., Ulbrich, I. M., Shields, L., Prather,
790 K., Hering, S., and Jimenez, J. L.: The influence of chemical composition and mixing state
791 of Los Angeles urban aerosol on CCN number and cloud properties, Atmos. Chem. Phys.,
792 8, 5649-5667, 10.5194/acp-8-5649-2008, 2008.

793 Dick, W. D., Saxena, P., and McMurry, P. H.: Estimation of water uptake by organic
794 compounds in submicron aerosols measured during the Southeastern Aerosol and
795 Visibility Study, Journal of Geophysical Research: Atmospheres (1984–2012), 105,
796 1471-1479, 2000.

Formatted: English (United States)

Formatted: EndNote Bibliography, Left

Formatted: Font: +Body (Cambria)

Formatted: English (United States)

797 Dusek, U., Reischl, G. P., and Hitzenberger, R.: CCN Activation of Pure and Coated Carbon
798 Black Particles, *Environmental Science & Technology*, 40, 1223-1230,
799 10.1021/es0503478, 2006.

800 Dusek, U., Frank, G. P., Massling, A., Zeromskiene, K., Iinuma, Y., Schmid, O., Helas, G.,
801 Hennig, T., Wiedensohler, A., and Andreae, M. O.: Water uptake by biomass burning
802 aerosol at sub- and supersaturated conditions: closure studies and implications for the
803 role of organics, *Atmos. Chem. Phys.*, 11, 9519-9532, 10.5194/acp-11-9519-2011, 2011.

804 Fast, J. D., Gustafson, W. I., Easter, R. C., Zaveri, R. A., Barnard, J. C., Chapman, E. G., Grell,
805 G. A., and Peckham, S. E.: Evolution of ozone, particulates, and aerosol direct radiative
806 forcing in the vicinity of Houston using a fully coupled meteorology-chemistry-aerosol
807 model, *Journal of Geophysical Research: Atmospheres*, 111, D21305,
808 10.1029/2005jd006721, 2006.

809 Frank, G., Martinsson, B. G., Cederfelt, S.-I., Berg, O. H., Swietlicki, E., Wendisch, M.,
810 Yuskiewicz, B., Heintzenberg, J., Wiedensohler, A., Orsini, D., Stratmann, F., Laj, P., and
811 Ricci, L.: Droplet Formation and Growth in Polluted Fogs, *Contrib. Atmos. Phys.*, 71, 65-
812 85, 1998.

813 Georgii, H. W., and Kleinjung, E.: Relations between the chemical composition of
814 atmospheric aerosol particles and the concentration of natural ice nuclei. , *J. Rech.*
815 *Atmos.*, 3, 145-156, 1967.

816 Ghan, S. J., Leung, L. R., Easter, R. C., and Abdul-Razzak, H.: Prediction of cloud droplet
817 number in a general circulation model, *Journal of Geophysical Research: Atmospheres*,
818 102, 21777-21794, 10.1029/97jd01810, 1997.

819 Grell, G. A., Peckham, S. E., Schmitz, R., McKeen, S. A., Frost, G., Skamarock, W. C., and
820 Eder, B.: Fully coupled "online" chemistry within the WRF model, *Atmospheric*
821 *Environment*, 39, 6957-6975, <http://dx.doi.org/10.1016/j.atmosenv.2005.04.027>,
822 2005.

823 Griffin, D. W., Kellogg, C. A., and Shinn, E. A.: Dust in the wind: Long range transport of
824 dust in the atmosphere and its implications for global public and ecosystem health,
825 *Global Change and Human Health*, 2, 20-33, 2001.

826 Hayes, T. P., Kinney, J. J. R., and Wheeler, N. J. M.: California surface wind climatology,
827 California Air Resources Board, Technical Support Division, Modeling and Meteorology
828 Branch, 1992.

829 Hong, S.-Y., Noh, Y., and Dudhia, J.: A New Vertical Diffusion Package with an Explicit
830 Treatment of Entrainment Processes, *Monthly Weather Review*, 134, 2318-2341,
831 10.1175/mwr3199.1, 2006.

832 Hong, S.-Y.: A new stable boundary-layer mixing scheme and its impact on the simulated
833 East Asian summer monsoon, *Quarterly Journal of the Royal Meteorological Society*,
834 136, 1481-1496, 10.1002/qj.665, 2010.

835 IPCC: Climate change 2007-the physical science basis: Working group I contribution to
836 the fourth assessment report of the IPCC, Cambridge University Press, 2007.

837 Joe, D. K., Zhang, H., DeNero, S. P., Lee, H.-H., Chen, S.-H., McDonald, B. C., Harley, R. A.,
838 and Kleeman, M. J.: Implementation of a high-resolution Source-Oriented WRF/Chem
839 model at the Port of Oakland, *Atmospheric Environment*, 82, 351-363,
840 <http://dx.doi.org/10.1016/j.atmosenv.2013.09.055>, 2014.

841 Kain, J. S., and Fritsch, J. M.: A one-dimensional entraining/detraining plume model and
842 its application in convective parameterization, *Journal of the atmospheric sciences*, 47,
843 2784-2802, 1990.

Formatted: Font: +Body (Cambria)

Formatted: English (United States)

Formatted: Font: +Body (Cambria)

Formatted: English (United States)

844 Kain, J. S.: Convective parameterization for mesoscale models: The Kain-Fritsch scheme,
845 The representation of cumulus convection in numerical models, Meteor. Monogr, 46,
846 165-170, 1993.

847 Kleeman, M. J., Cass, G. R., and Eldering, A.: Modeling the airborne particle complex as a
848 source-oriented external mixture, Journal of Geophysical Research-Atmospheres, 102,
849 21355-21372, 10.1029/97jd01261, 1997.

850 Koch, D., and Del Genio, A. D.: Black carbon semi-direct effects on cloud cover: review
851 and synthesis, Atmos. Chem. Phys., 10, 7685-7696, 10.5194/acp-10-7685-2010, 2010.

852 Lance, S., Raatikainen, T., Onasch, T. B., Worsnop, D. R., Yu, X. Y., Alexander, M. L.,
853 Stolzenburg, M. R., McMurry, P. H., Smith, J. N., and Nenes, A.: Aerosol mixing state,
854 hygroscopic growth and cloud activation efficiency during MIRAGE 2006, Atmos. Chem.
855 Phys., 13, 5049-5062, 10.5194/acp-13-5049-2013, 2013.

856 Lesins, G., Chylek, P., and Lohmann, U.: A study of internal and external mixing scenarios
857 and its effect on aerosol optical properties and direct radiative forcing, Journal of
858 Geophysical Research-Atmospheres, 107, 10.1029/2001jd000973, 2002.

859 Li, W. J., and Shao, L. Y.: Observation of nitrate coatings on atmospheric mineral dust
860 particles, Atmos. Chem. Phys., 9, 1863-1871, 10.5194/acp-9-1863-2009, 2009.

861 Lin, Y.-L., Farley, R. D., and Orville, H. D.: Bulk Parameterization of the Snow Field in a
862 Cloud Model, Journal of Climate and Applied Meteorology, 22, 1065-1092, 1983.

863 Liu, Y., Daum, P. H., and McGraw, R. L.: Size truncation effect, threshold behavior, and a
864 new type of autoconversion parameterization, Geophysical Research Letters, 32,
865 L11811, 10.1029/2005gl022636, 2005.

866 Lohmann, U., and Feichter, J.: Global indirect aerosol effects: a review, Atmos. Chem.
867 Phys., 5, 715-737, 10.5194/acp-5-715-2005, 2005.

868 [Ma, J., Chen, Y., Wang, W., Yan, P., Liu, H., Yang, S., Hu, Z., and Lelieveld, J.: Strong air
869 pollution causes widespread haze-clouds over China, Journal of Geophysical Research:
870 Atmospheres, 115, n/a-n/a, 10.1029/2009JD013065, 2010.](#)

871 [McMichael, A. J., Woodruff, R. E., and Hales, S.: Climate change and human health:
872 present and future risks, The Lancet, 367, 859-869, 2006.](#)

873 Ming, Y., and Russell, L. M.: Organic aerosol effects on fog droplet spectra, Journal of
874 Geophysical Research: Atmospheres, 109, D10206, 10.1029/2003jd004427, 2004.

875 Moore, K. F., Sherman, D. E., Reilly, J. E., and Collett, J. L.: Drop size-dependent chemical
876 composition in clouds and fogs. Part I. Observations, Atmospheric Environment, 38,
877 1389-1402, <http://dx.doi.org/10.1016/j.atmosenv.2003.12.013>, 2004.

878 Motoi, K.: Electron-microscope study of snow crystal nuclei, Journal of Meteorology, 8,
879 151-156, 1951.

880 Niu, S. J., Liu, D. Y., Zhao, L. J., Lu, C. S., Lü, J. J., and Yang, J.: Summary of a 4-Year Fog Field
881 Study in Northern Nanjing, Part 2: Fog Microphysics, Pure and Applied Geophysics, 169,
882 1137-1155, 10.1007/s00024-011-0344-9, 2012.

883 Ramanathan, V., Crutzen, P. J., Kiehl, J. T., and Rosenfeld, D.: Atmosphere - Aerosols,
884 climate, and the hydrological cycle, Science, 294, 2119-2124, 10.1126/science.1064034,
885 2001.

886 Rogers, R. R., and Yau, M. K.: A Short Course in Cloud Physics, Third ed., Butterworth
887 Heinemann, 1989.

888 Schell, B., Ackermann, I. J., Hass, H., Binkowski, F. S., and Ebel, A.: Modeling the formation
889 of secondary organic aerosol within a comprehensive air quality model system, Journal
890 of Geophysical Research: Atmospheres (1984–2012), 106, 28275-28293, 2001.

Formatted: English (United States)

Formatted: English (United States)

Formatted: EndNote Bibliography, Left

Formatted: Font: +Body (Cambria)

Formatted: English (United States)

891 Skamarock, W. C., Klemp, J. B., Dudhia, J., Gill, D. O., Barker, D. M., Duda, M. G., Huang, X.-
892 Y., Wang, W., and Powers, J. G.: A Description of the Advanced Research WRF Version 3,
893 NCAR Technical Note, NCAR/TN-475+STR, 2008.
894 Stelson, A. W.: Urban aerosol refractive index prediction by partial molar refraction
895 approach, *Environmental Science & Technology*, 24, 1676-1679, 10.1021/es00081a008,
896 1990.
897 Sullivan, R. C., Petters, M. D., DeMott, P. J., Kreidenweis, S. M., Wex, H., Niedermeier, D.,
898 Hartmann, S., Clauss, T., Stratmann, F., Reitz, P., Schneider, J., and Sierau, B.: Irreversible
899 loss of ice nucleation active sites in mineral dust particles caused by sulphuric acid
900 condensation, *Atmospheric Chemistry and Physics*, 10, 11471-11487, 10.5194/acp-10-
901 11471-2010, 2010.
902 Tegen, I., Lacis, A. A., and Fung, I.: The influence on climate forcing of mineral aerosols
903 from disturbed soils, *Nature*, 380, 419-422, 10.1038/380419a0, 1996.
904 Tewari, M., Chen, F., Kusaka, H., and Miao, S.: Coupled WRF/Unified Noah/urban-canopy
905 modeling system, NCAR WRF Documentation, NCAR, Boulder, 1-22, 2007.
906 Twomey, S.: POLLUTION AND PLANETARY ALBEDO, *Atmospheric Environment*, 8,
907 1251-1256, 10.1016/0004-6981(74)90004-3, 1974.
908 Yang, F.: Radiative forcing and climate impact of the Mount Pinatubo volcanic eruption. ,
909 PhD, University of Illinois at Urbana-Champaign., 2000.
910 Yang, M., Howell, S. G., Zhuang, J., and Huebert, B. J.: Attribution of aerosol light
911 absorption to black carbon, brown carbon, and dust in China – interpretations of
912 atmospheric measurements during EAST-AIRE, *Atmos. Chem. Phys.*, 9, 2035-2050,
913 10.5194/acp-9-2035-2009, 2009.
914 Ying, Q., and Kleeman, M. J.: Effects of aerosol UV extinction on the formation of ozone
915 and secondary particulate matter, *Atmospheric Environment*, 37, 5047-5068, 2003.
916 Ying, Q., Lu, J., Allen, P., Livingstone, P., Kaduwela, A., and Kleeman, M.: Modeling air
917 quality during the California Regional PM10/PM2.5 Air Quality Study (CRPAQS) using
918 the UCD/CIT source-oriented air quality model - Part I. Base case model results,
919 *Atmospheric Environment*, 42, 8954-8966, DOI 10.1016/j.atmosenv.2008.05.064, 2008.
920 Zaveri, R. A., Easter, R. C., Fast, J. D., and Peters, L. K.: Model for Simulating Aerosol
921 Interactions and Chemistry (MOSAIC), *Journal of Geophysical Research: Atmospheres*,
922 113, D13204, 10.1029/2007jd008782, 2008.
923 Zaveri, R. A., Barnard, J. C., Easter, R. C., Riemer, N., and West, M.: Particle-resolved
924 simulation of aerosol size, composition, mixing state, and the associated optical and
925 cloud condensation nuclei activation properties in an evolving urban plume, *Journal of*
926 *Geophysical Research: Atmospheres*, 115, D17210, 10.1029/2009jd013616, 2010.
927 Zhang, H., DeNero, S. P., Joe, D. K., Lee, H. H., Chen, S. H., Michalakes, J., and Kleeman, M.
928 J.: Development of a source oriented version of the WRF/Chem model and its
929 application to the California regional PM10 / PM2.5 air quality study, *Atmos. Chem.*
930 *Phys.*, 14, 485-503, 10.5194/acp-14-485-2014, 2014.
931

932

933

934 **Captions of Tables**

935 Table 1. Chemical species that are carried in the AQC/CLDAQ “species” dimension. All
936 species are in concentrations ($\mu\text{g m}^{-3}$) except for the last two elements (i.e., 39 and
937 40), which carry the number concentration ($\# \text{m}^{-3}$) and radius (m).

938 Table 2. California Ambient Air Quality Data (CAAQD) station information.

939 Table 3. Numerical experiment designs for this study.

940 Table 4. Hourly bias mean and standard deviation (std) in day time and night time of 2-m
941 temperature (T_2 , $^{\circ}\text{C}$), water vapor mixing ratio (Q_2 , g kg^{-1}), and net downward
942 shortwave radiative flux (NSF, W m^{-2}) between all experiments and observation from
943 16 to 18 January 2011. T_2 and Q_2 are calculated using 24 surface stations and NSF is
944 calculated using 42 CIMIS stations shown in Fig. 4.

945 Table 5. Mean values of cloud liquid water-mixing ratio (Q_c), cloud droplet number (Q_n),
946 surface skin temperature (SKT), net shortwave flux (NSF), latent heat flux (LH) and
947 sensible heat flux (SH) for four experiments over the entire Central Valley during 16
948 to 18 January 2011.

949 Table 6. ~~Ratio~~The ratio of AQC number concentration for each bin/source to the total number
950 concentration. The numbers are averaged within the first five model layers during 16
951 to 18 January 2011.

952 Table 7. Hourly bias mean and root-mean-square-difference of cloud liquid water-mixing
953 ratio (Q_c), cloud droplet number (Q_n), surface skin temperature (SKT), net shortwave
954 flux (NSF), latent heat flux (LH) and sensible heat flux (SH) between internally
955 mixed (I_ARon_CRmod) and source-oriented (S_ARon_CRmod) experiments
956 (internally mixed – source-oriented) during 16 to 18 January 2011.

957
958

959 **Captions of Figures**

960 Figure 1. Cloud physics processes that are involved with cloud particles in the SOWC model
961 with a 6D aerosol variable (AQC) and a 6D cloud variable (CLDAQC) included.
962 Black solid arrow and grey dashed arrow indicate the source and the sink processes of
963 cloud water and 6D CLDAQC, as well as 6D AQC, respectively.

964 Figure 2. MODIS true color image at (a) 1930 UTC 16 January 2011 and (b) 1835 UTC 17
965 January 2011 from Satellite Terra, respectively.

966 Figure 3. The column integrated water vapor (shaded; mm), 850-hPa wind vector, and sea
967 level pressure (contours; hPa) from ECMWF Interim reanalysis at (a) 0000 UTC (4
968 pm local time) 11 January, (b) 0000 UTC 12 January, (c) 0000 UTC 13 January, (d)
969 0000 UTC 14 January, (e) 0000 UTC 15 January, (f) 0000 UTC 16 January, (g) 0000
970 UTC 17 January, and (h) 0000 UTC 18 January, 2011.

971 Figure 4. NOAA's National Climatic Data Center (NCDC; 24 stations, red dots), California
972 Irrigation Management Information System (CIMIS; 42 stations, black dots) and
973 California Ambient Air Quality Data (6 stations, numbers corresponding to Table 2
974 station ID) measurement locations. Shaded is terrain height in m.

975 Figure 5. The 72-hour averaged (16 to 18 January 2011) AQC number concentration
976 averaged over the first five model layers from the polluted experiment
977 (S_ARon_CRmod) in units of $10^8 \# m^{-3}$. Contours are terrain heights in m.

978 Figure 6. Comparison of (a) Nitrate (NO_3^-), (b) Sulfate (SO_4^{2-}), (c) Ammonium (NH_4^+), and
979 (d) Soluble Sodium (Na^+) between simulated source-oriented experiment
980 (S_ARon_CRmod), internally mixed experiment (I_ARon_CRmod) and the observed
981 concentrations of airborne particles on 18 January 2011. Units are $\mu g m^{-3}$.

982 Figure 7. Liquid water path (LWP) ($g m^{-2}$) from MODIS Level 2 cloud products ((a), (c) and

983 (e)) and from the SOWC model with aerosol feedback on and modified cloud-
984 radiation scheme (S_ARon_CRmod; (b), (d) and (ef)). (a) and (b) are at 1900 UTC 16
985 January 2011. (c) and (d) are at 1800 UTC 17 January 2011. (e) and (f) are at 1900
986 UTC 18 January 2011. Contours in (b), (d) and (ef) are terrain heights in m.

987 Figure 8. Same as Figure 5 but cloud optical thickness (COT) (dimensionless).

988 Figure 9. Mean bias variation of (a) 2-m temperature (T2), (b) 2-m water vapor mixing ratio
989 (Q2), and (c) surface net downward shortwave radiative flux (NSF) between
990 observations and model simulation from 16 to 18 January 2011 for S_ARon_CRmod
991 (blue lines), S_ARoff_CRmod (purple lines) and I_ARon_CRmod (red lines)
992 experiments.

993 Figure 10. N_{CCN}/N_{CN} ratio for (a) S_ARon_CRmod (source-oriented experiment) and (b)
994 I_ARon_CRmod (internally mixed experiment) averaged within the first five model
995 layers. The ratio is hourly average during 16 to 18 January 2011. Contours are
996 terrain heights in m.

997 Figure 11. (a) 72-hour averaged CCN concentration at supersaturation of 0.02%, 0.05%,
998 0.1%, 0.2%, 0.5% and total AQC concentration with units in $\# \text{ cm}^{-3}$. (b) N_{CCN}/N_{CN}
999 ratio at 5 corresponding supersaturation. Dark gray is source-oriented experiment and
1000 light gray represents internally mixed experiment. Results are average values using
1001 data within the first five model layers.

1002 Figure 12. Relative change $((\text{internally mixed} - \text{source-oriented})/\text{source-oriented} * 100\%)$ in
1003 72-hour averaged predictions during 16 to 18 January 2011 for (a) the ratio of cloud
1004 liquid water mixing ratio, (b) cloud droplet number, (c) surface skin temperature and
1005 (d) net shortwave radiation. (a) and (b) are average values using data within the first
1006 five model layers. Contours are terrain heights in m.

1007 Figure 13. Area average of latent heat flux (LH) and sensible heat flux (SH) over the Central

1008 Valley in S_ARon_CRmod and the average difference between I_ARon_CRmod and
1009 S_ARon_CRmod from 0800 UTC 17 January (00 Z local time) to 0700 UTC 18 January
1010 (23 Z local time).

1011

1012

1013 Table 1. Chemical species that are carried in the AQC/CLDAQC “species” dimension. All
 1014 species are in concentrations ($\mu\text{g m}^{-3}$) except for the last two elements (i.e., 39 and 40), which
 1015 carry the number concentration ($\# \text{m}^{-3}$) and radius (m).

	Chemical species		Chemical species
1	EC	21	SOA from lumped Alkane 1
2	OC	22	SOA from lumped Alkane 2
3	NA	23	SOA from lumped Aromatic 1
4	CL	24	SOA from lumped Aromatic 2
5	N3	25	SOA from lumped Aromatic 1
6	S6	26	SOA from lumped Aromatic 2
7	N5	27	SOA from lumped Aromatic 1
8	Other	28	SOA from lumped Aromatic 2
9	Metal	29	SOA from lumped Alkene 1
10	Unknown	30	SOA from lumped Alkene 2
11	CU1	31	SOA from lumped Alpha Pinene 1
12	CU2	32	SOA from lumped Alpha Pinene 2
13	MN2	33	SOA from lumped Beta Pinene 1
14	MN3	34	SOA from lumped Beta Pinene 2
15	FE2	35	SOA from lumped Toluene 1
16	FE3	36	SOA from lumped Toluene 2
17	S4	37	Hydrogen Ion
18	Air (hollow sea salt particles)	38	Water
19	NO3	39	Number Concentration
20	Non-explicit SOA	40	Particle Mean Volume Radius

1016

1017

1018

1019

1020

1021

1022

1023

1024

Table 2. California Ambient Air Quality Data (CAAQD) station information

Station ID	Station name	Longitude (°)	Latitude (°)
1	San Jose-Jackson Street	-121.89	37.35
2	Bakersfield-5558 Cal. Avenue	-119.06	35.36
3	Fresno-1st Street	-119.77	36.78
4	Modesto-14th Street	-120.99	37.64
5	Visalia-N Church Street	-119.29	36.33
6	Sacramento-T Street	-121.49	38.57

Formatted Table

1025

1026

Table 3. Numerical experiment designs for this study.

Experiments	Description
S_ARon_CRmod	Source-Oriented aerosols with aerosol direct effect calculation on and modified cloud radiation parameterization
S_ARon_CRorig	Source-Oriented aerosols with aerosol direct effect calculation on and original cloud radiation parameterization
S_ARoff_CRmod	Source-Oriented aerosols with aerosol direct effect calculation off and modified cloud radiation parameterization
I_ARon_CRmod	Internal mixing aerosols with aerosol direct effect calculation on and modified cloud radiation parameterization

1027

1028 Table 4. Hourly bias mean and standard deviation (std) in day time and night time of 2-m
 1029 temperature (T2, °C), water vapor mixing ratio (Q2, g kg-air⁻¹), and net downward shortwave
 1030 radiative flux (NSF, W m⁻²) between all experiments and observation from 16 to 18 January
 1031 2011. T2 and Q2 are calculated using 24 surface stations and NSF is calculated using 42
 1032 CIMIS stations shown in Fig. 4.

	S_ARon_CRmod		S_ARon_CRorig		S_ARoff_CRmod		I_ARon_CRmod	
Daytime	Bias mean	std	Bias mean	std	Bias mean	std	Bias mean	std
T2	-1.76	1.27	-1.72	1.32	-1.63	1.33	-2.01	1.09
Q2	-0.56	0.34	-0.56	0.36	-0.54	0.35	-0.57	0.32
NSF	13.91	53.18	14.40	58.00	18.81	58.78	8.68	50.03
Nighttime	Bias mean	std	Bias mean	std	Bias mean	std	Bias mean	std
T2	-2.22	0.92	-2.21	0.95	-2.19	0.93	-2.30	0.87
Q2	-0.88	0.41	-0.87	0.42	-0.88	0.42	-0.89	0.41
NSF	/	/	/	/	/	/	/	/

1033
 1034

1035
1036 Table 5. Mean values of cloud liquid water-mixing-ratio (Q_c), cloud droplet number (Q_n),
1037 surface skin temperature (SKT), net shortwave flux (NSF), latent heat flux (LH) and sensible
1038 heat flux (SH) for four experiments over the entire Central Valley during 16 to 18 January
1039 2011.
1040

	S_ARon_CRmod	S_ARon_CRorig	S_ARoff_CRmod	I_ARon_CRmod
Q_c^* (g m^{-3})	0.220	0.221	0.213	0.231
Q_n^* ($\# \text{m}^{-3}$)	3.94×10^8	4.18×10^8	3.77×10^8	4.57×10^8
SKT (K)	281.305	281.30	281.404	281.151
NSF** (W m^{-2})	130.56	131.02	134.24	124.54
LH (W m^{-2})	9.01	9.02	9.36	8.40
SH (W m^{-2})	4.91	4.55	5.27	4.54
COT (unitless)	25.56	25.15	24.49	28.62

1041 * Averaged within the first five model layers

1042 ** Averaged only in the daytime

1043

1044 Table 6. Ratio of AQC number concentration for each bin/source to the total number
1045 concentration. The numbers are averaged within the first five model layers during 16 to 18
1046 January 2011.

Formatted: Justified

	Wood smoke	Gasoline	Diesel	Meat cooking	Others	Source- oriented	Internal
Bin1	28.92%	1.00%	4.25%	0.84%	10.39%	45.40%	48.89%
Bin2	9.12%	0.38%	1.48%	0.60%	38.64%	50.22%	46.74%
Bin3	0.19%	0.01%	0.03%	0.02%	3.03%	3.28%	3.26%
Bin4	0.00%	0.00%	0.00%	0.00%	0.17%	0.18%	0.21%
Bin5	0.00%	0.00%	0.00%	0.00%	0.02%	0.02%	0.02%
Bin6	0.00%	0.00%	0.00%	0.00%	0.00%	0.00%	0.00%
Bin7	0.00%	0.00%	0.00%	0.00%	0.00%	0.00%	0.00%
Bin8	0.00%	0.00%	0.00%	0.00%	0.91%	0.91%	0.88%

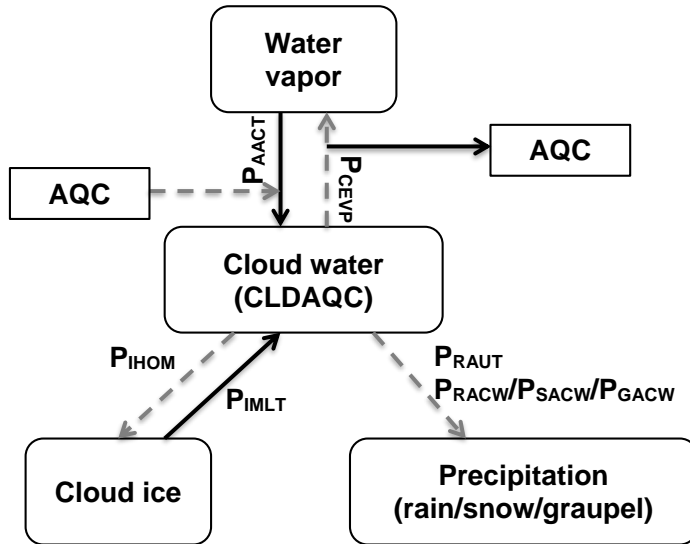
1047

1048 Table 7. Hourly bias mean and root-mean-square-difference of cloud liquid water ~~mixing~~
 1049 ~~ratio~~ (Q_c), cloud droplet number (Q_n), surface skin temperature (SKT), net shortwave flux
 1050 (NSF), latent heat flux (LH) and sensible heat flux (SH) between internally mixed
 1051 (I_ARon_CRmod) and source-oriented (S_ARon_CRmod) experiments (internally mixed –
 1052 source-oriented) during 16 to 18 January 2011.

	Bias mean	Root-mean-square-difference
Q_c^* (g m^{-3})	1.19×10^{-2}	4.16×10^{-2}
Q_n^* ($\# \text{ m}^{-3}$)	6.24×10^7	2.64×10^8
SKT (K)	-0.15	0.57
NSF (W m^{-2})	-6.02	13.30
LH (W m^{-2})	-0.61	2.75
SH (W m^{-2})	-0.36	5.24

1053 * Averaged within the first five model layers

1054
1055
1056



1057
1058
1059
1060
1061
1062
1063
1064

Figure 1. Cloud physics processes that are involved with cloud particles in the SOWC model with a 6D aerosol variable (AQC) and a 6D cloud variable (CLDAQC) included. Black solid arrow and grey dashed arrow indicate the source and the sink processes of cloud water and 6D CLDAQC, as well as 6D AQC, respectively.

1065
1066
1067
1068
1069
1070
1071
1072
1073
1074
1075
1076
1077
1078
1079
1080
1081
1082
1083
1084
1085
1086
1087
1088
1089
1090
1091
1092
1093
1094
1095
1096
1097
1098
1099
1100
1101
1102
1103
1104
1105
1106

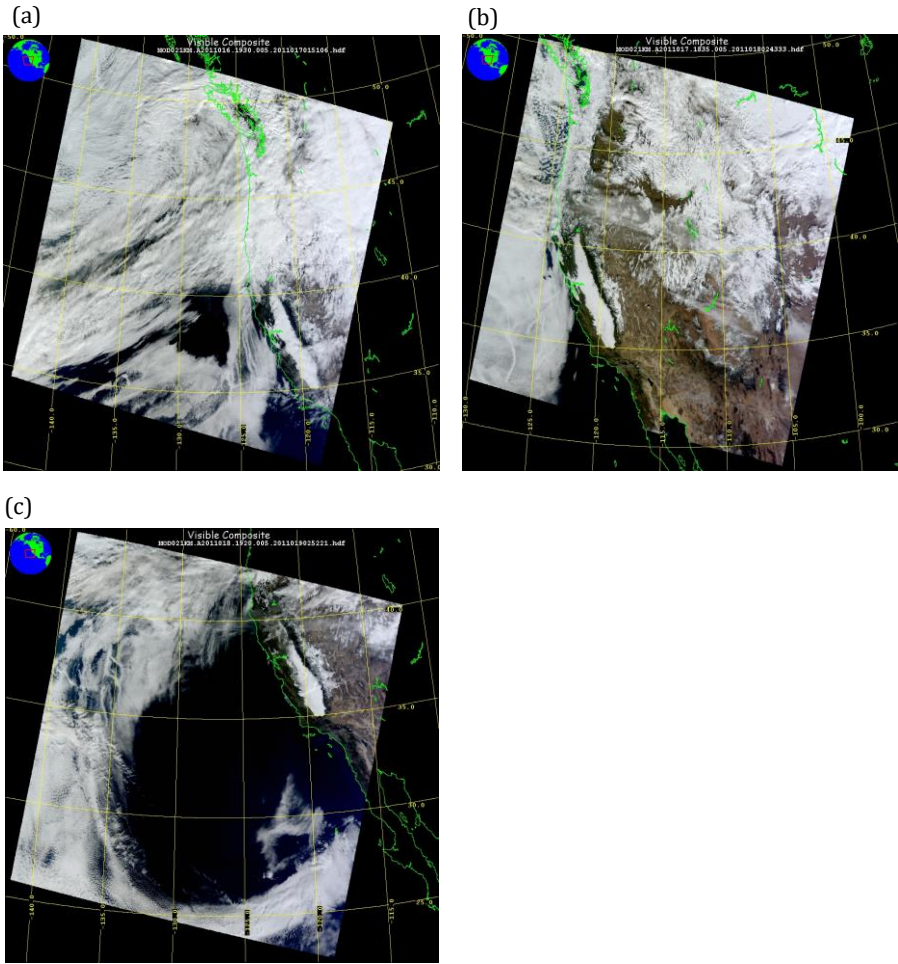


Figure 2. MODIS true color images at (a) 1930 UTC 16 January, (b) 1835 UTC 17 January, and (c) 1920 UTC 18 January, 2011 from Satellite Terra.

1107
1108
1109
1110
1111
1112
1113
1114
1115
1116
1117
1118
1119
1120
1121
1122
1123
1124
1125
1126
1127
1128
1129
1130
1131
1132
1133
1134
1135
1136
1137
1138
1139
1140
1141
1142
1143
1144
1145
1146
1147
1148
1149
1150
1151
1152
1153
1154
1155
1156

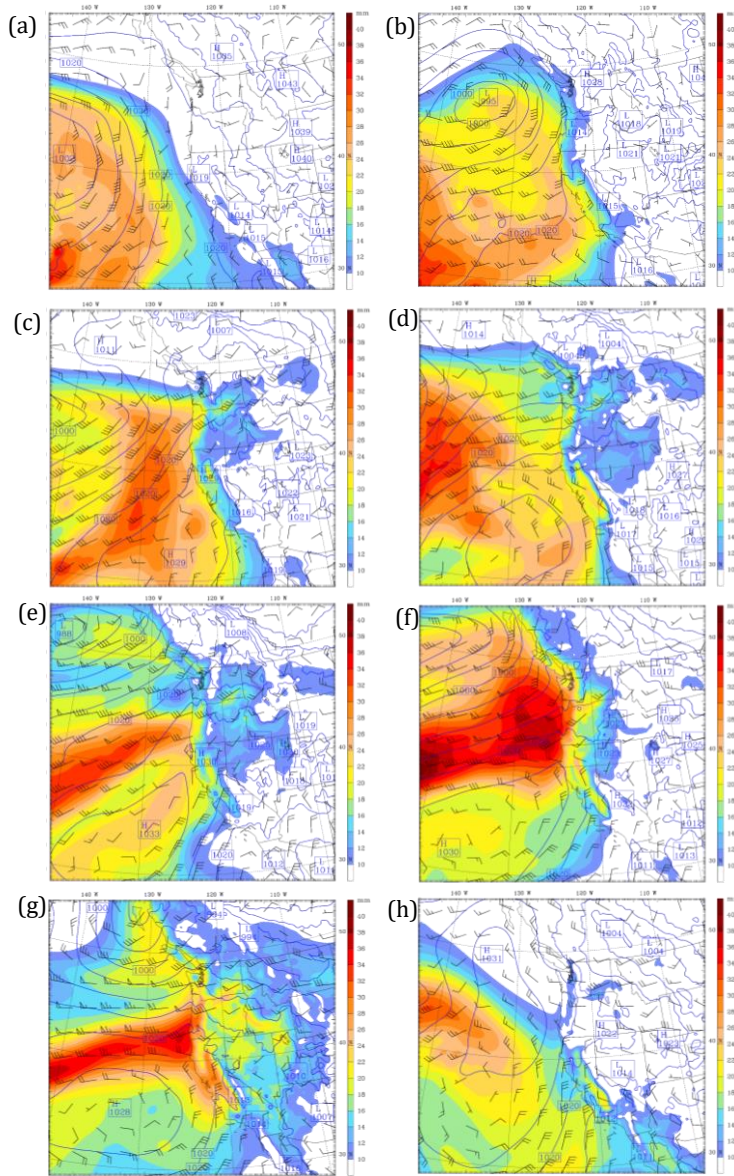
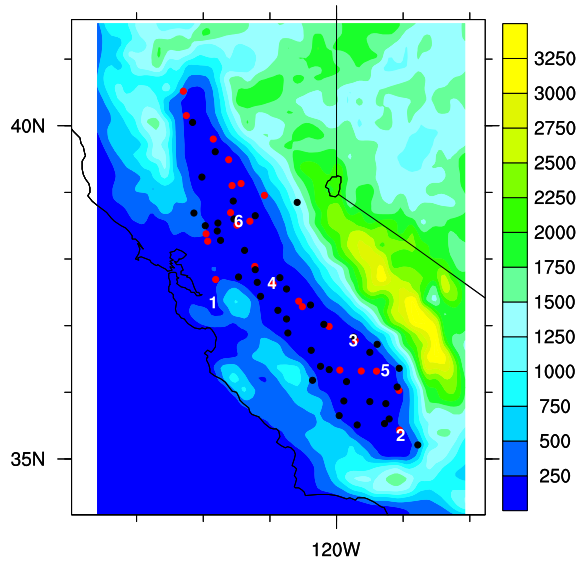
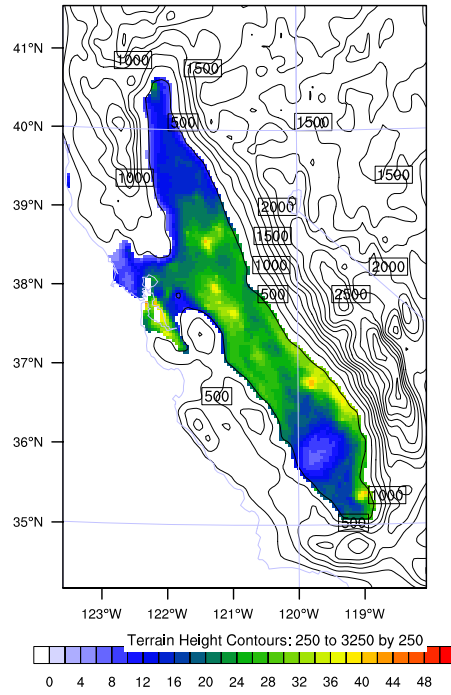


Figure 3. The column integrated water vapor (shaded; mm), 850-hPa wind vector, and sea level pressure (contours; hPa) from ECMWF Interim reanalysis at (a) 0000 UTC (4 pm local time) 11 January, (b) 0000 UTC 12 January, (c) 0000 UTC 13 January, (d) 0000 UTC 14 January, (e) 0000 UTC 15 January, (f) 0000 UTC 16 January, (g) 0000 UTC 17 January, and (h) 0000 UTC 18 January, 2011.



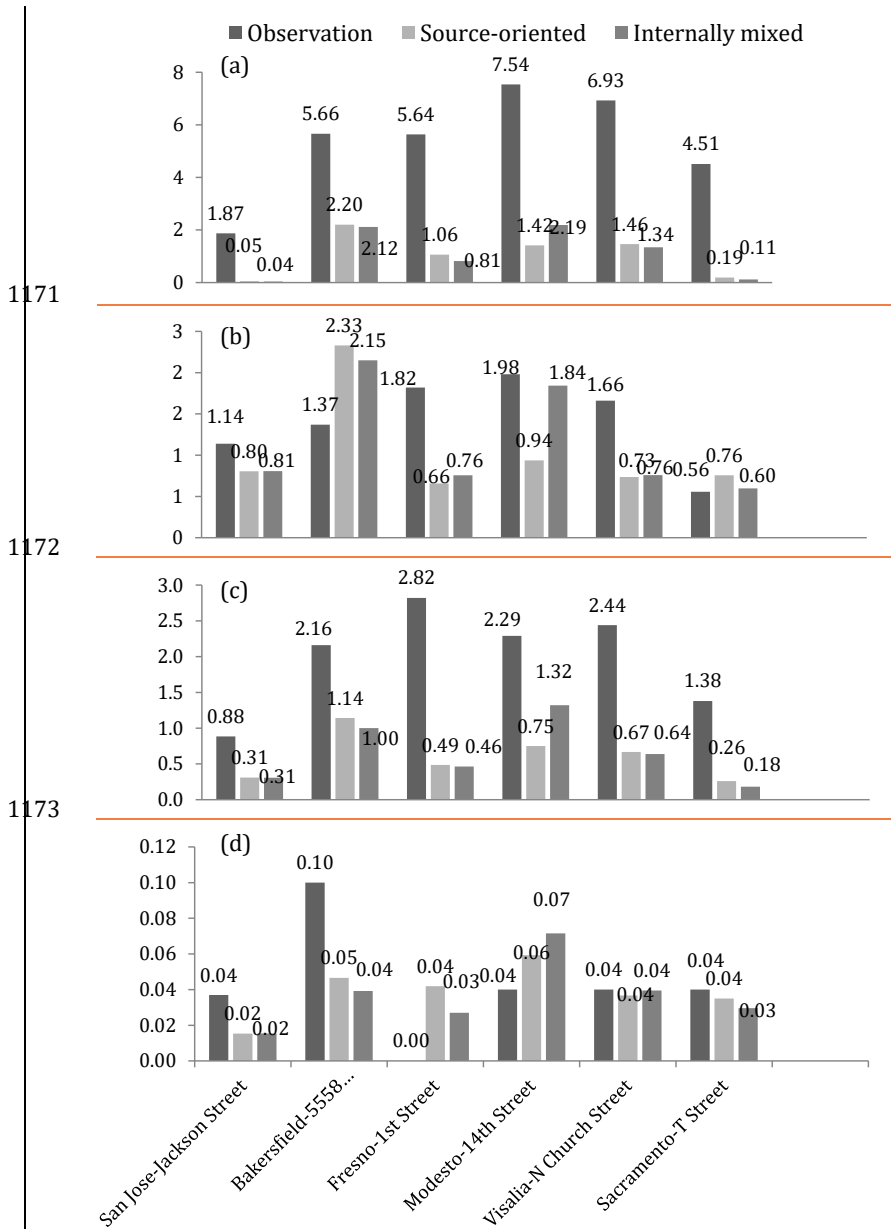
1157
 1158 Figure 4. NOAA's National Climatic Data Center (NCDC; 24 stations, red dots), California
 1159 Irrigation Management Information System (CIMIS; 42 stations, black dots) and California
 1160 Ambient Air Quality Data (6 stations, numbers corresponding to Table 2 station ID)
 1161 measurement locations. Shaded is terrain height in m.

1162
1163
1164
1165



1166
1167
1168
1169
1170

Figure 5. The 72-hour averaged (16 to 18 January 2011) AQ number concentration averaged over the first five model layers from the experiment S_ARon_CRmod in units of $10^8 \# \text{ m}^{-3}$. Contours are terrain heights in m.



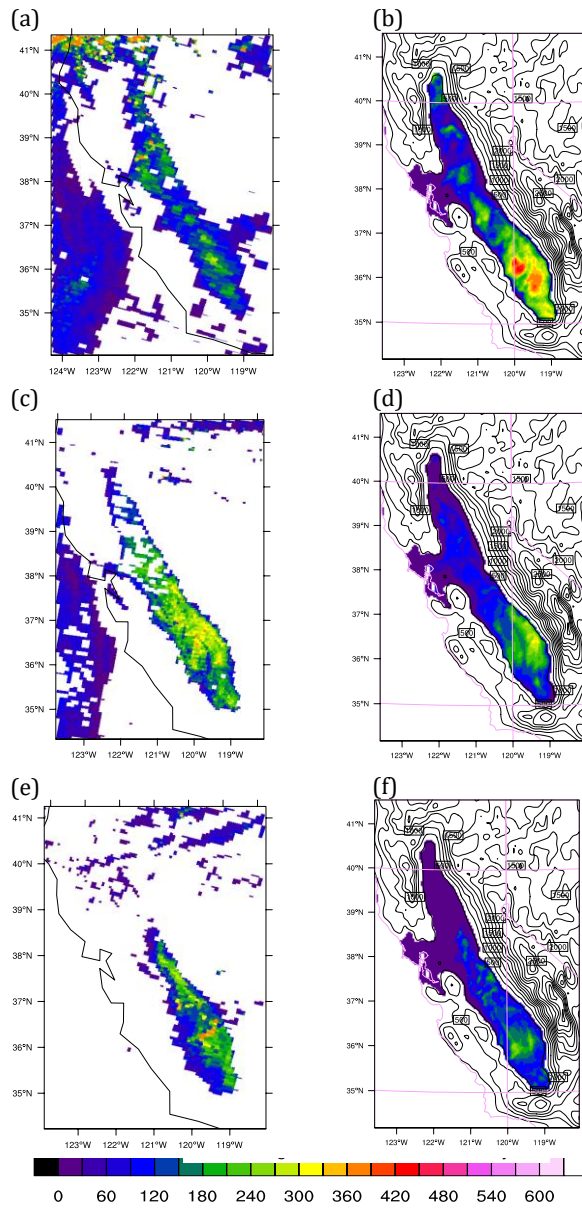
1174
 1175
 1176 Figure 6. Comparison of (a) Nitrate (NO_3^-), (b) Sulfate (SO_4^{2-}), (c) Ammonium (NH_4^+), and
 1177 (d) Soluble Sodium (Na^+) between simulated source-oriented experiment (S_ARon_CRmod),
 1178 internally mixed experiment (I_ARon_CRmod) and the observed concentrations of airborne
 1179 particles on 18 January 2011. Units are $\mu\text{g m}^{-3}$.

1180
1181

1182
1183

1184
1185

1186
1187
1188



1189
1190
1191
1192
1193

Figure 7. Liquid water path (LWP) (g m^{-2}) from MODIS Level 2 cloud products ((a), (c) and (e)) and from the SOWC model with aerosol feedback on and modified cloud-radiation scheme (S_ARon_CRmod; (b), (d) and (ef)). (a) and (b) are at 1900 UTC 16 January 2011. (c) and (d) are at 1800 UTC 17 January 2011. (e) and (f) are at 1900 UTC 18 January 2011. Contours in (b), (d) and (ef) are terrain heights in m.

1194
1195
1196

1197
1198

1199
1200

1201

1202
1203
1204
1205
1206

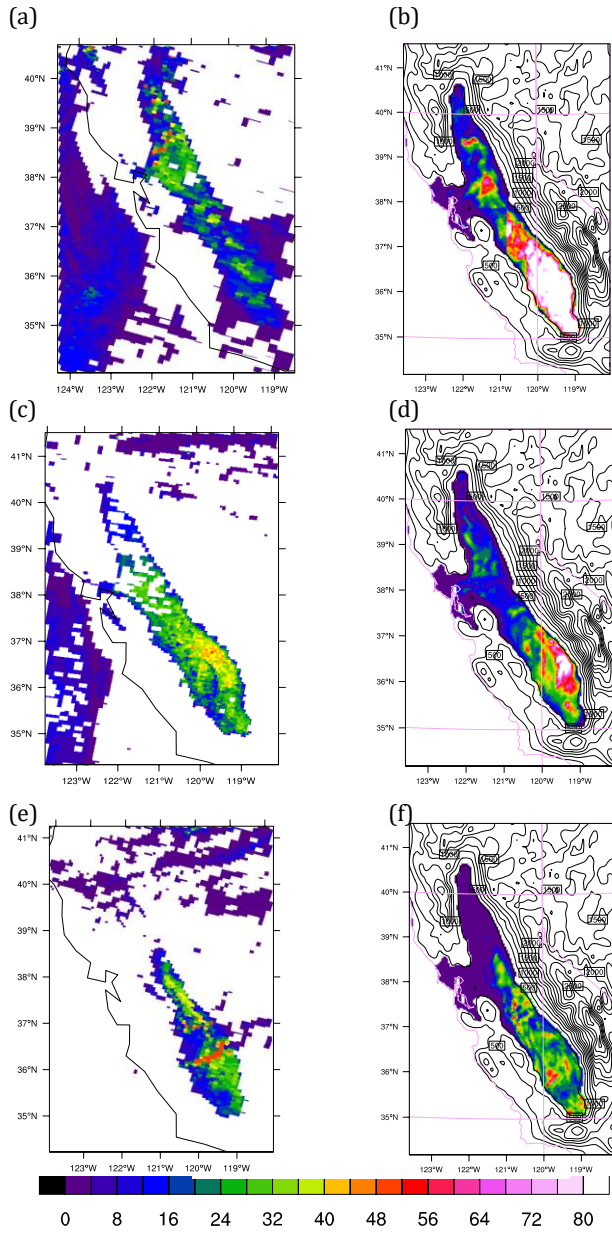


Figure 8. Same as Figure 5 but cloud optical thickness (COT) (dimensionless).

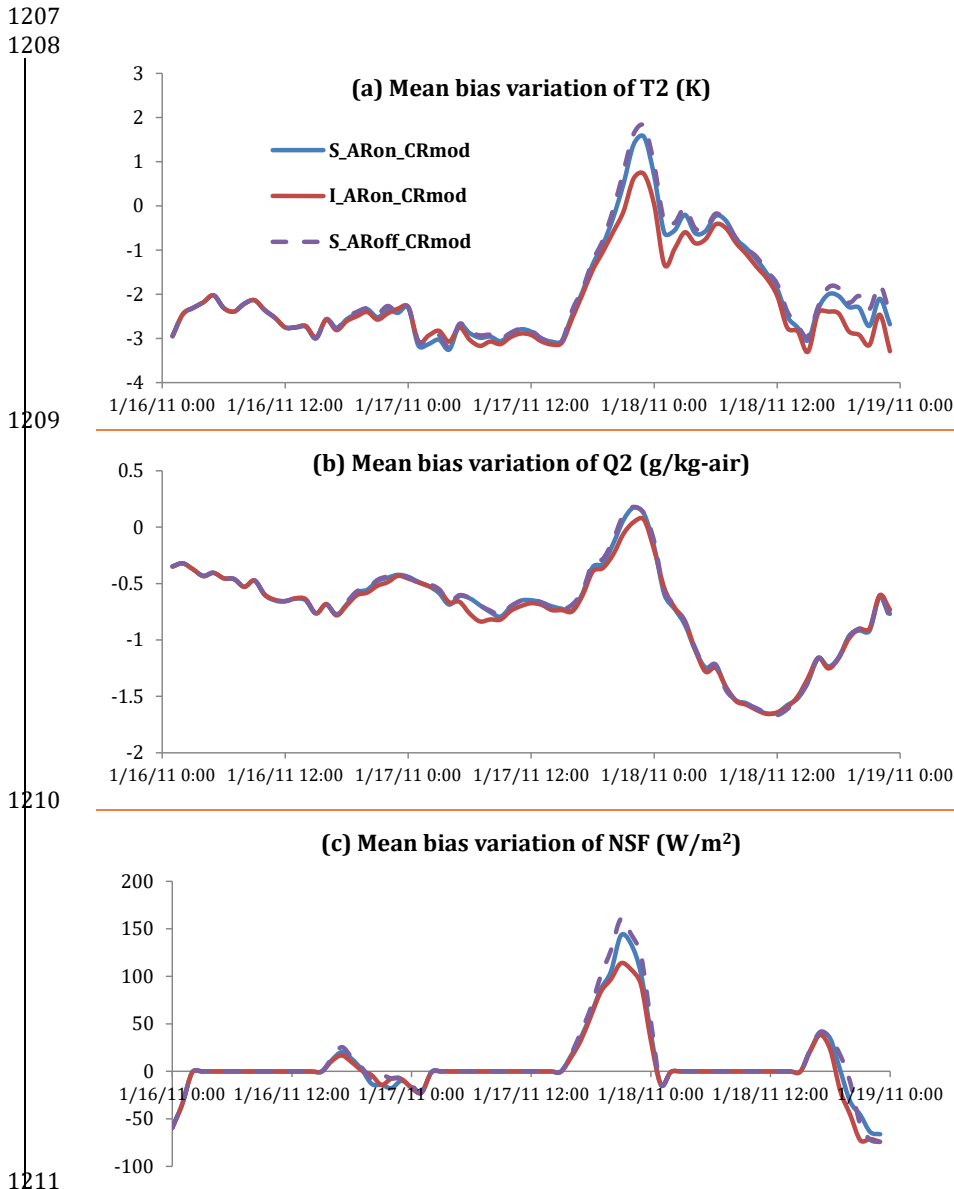
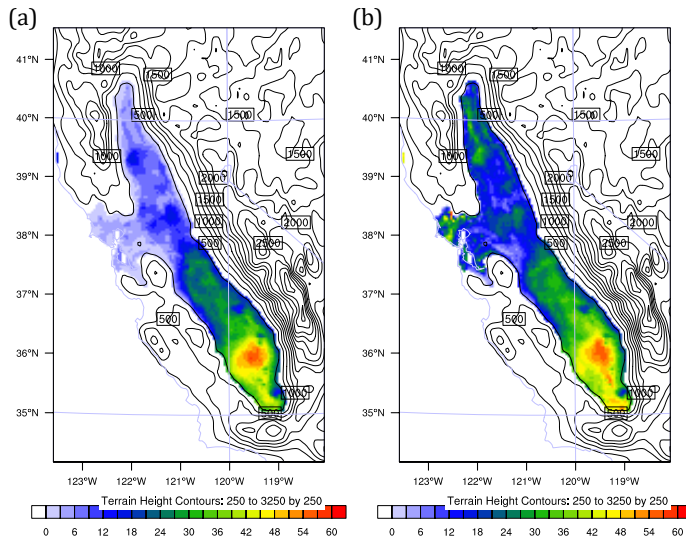


Figure 9. Mean bias variation of (a) 2-m temperature (T2), (b) 2-m water vapor mixing ratio (Q2), and (c) surface net downward shortwave radiative flux (NSF) between observations and model simulation from 16 to 18 January 2011 for S_ARon_CRmod (blue lines), S_ARoff_CRmod (purple lines) and I_ARon_CRmod (red lines) experiments.

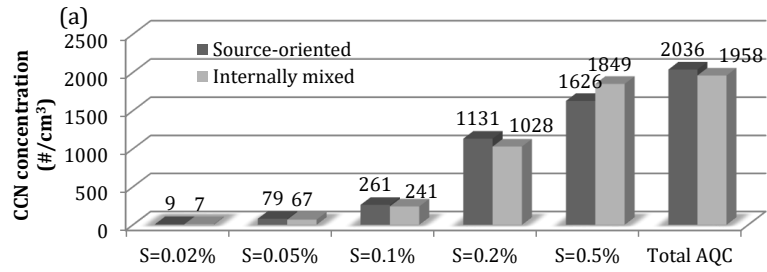
1217
1218
1219



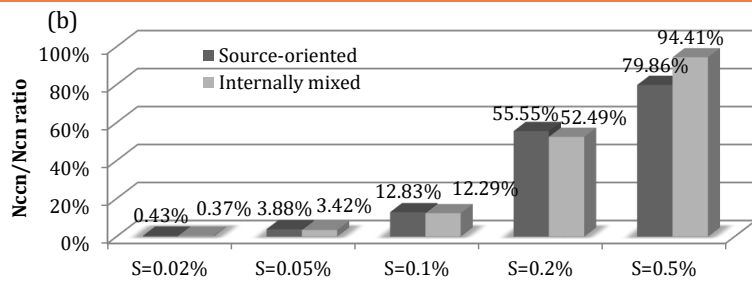
1220
1221
1222
1223
1224
1225
1226

Figure 10. $NCCN/NCN$ ratio for (a) S_ARon_CRmod (source-oriented experiment) and (b) I_ARon_CRmod (internally mixed experiment) averaged within the first five model layers. The ratio is hourly average during 16 to 18 January 2011. Contours are terrain heights in m.

1227



1228

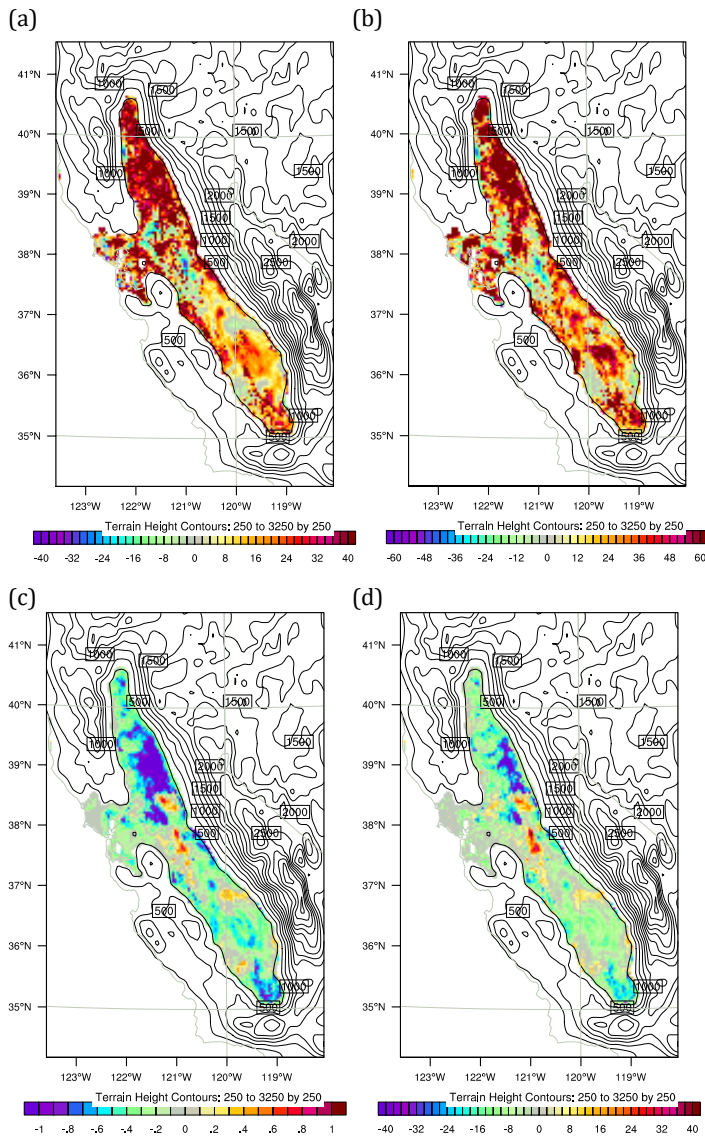


1229

1230

1231 Figure 11. (a) 72-hour averaged CCN concentration at supersaturation of 0.02%, 0.05%,
 1232 0.1%, 0.2%, 0.5% and total AQC concentration with units in $\# \text{cm}^{-3}$. (b) $N_{\text{CCN}}/N_{\text{CN}}$ ratio at 5
 1233 corresponding supersaturation. Dark gray is source-oriented experiment and light gray
 1234 represents internally mixed experiment. Results are average values using data within the first
 1235 five model layers.

1236
1237
1238

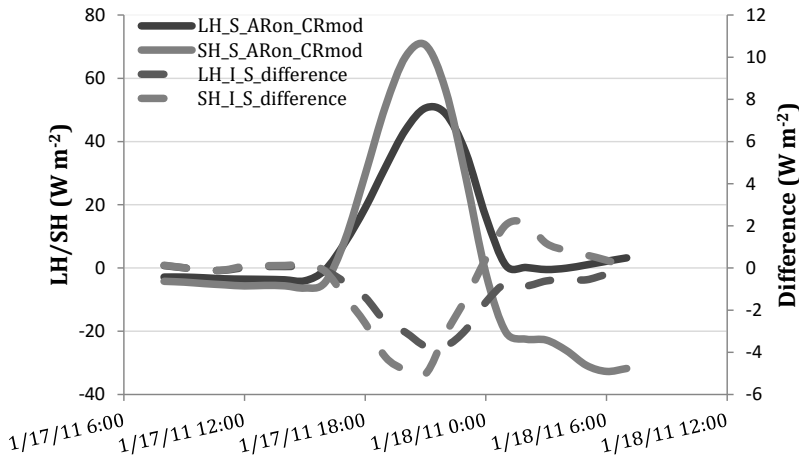


1239
1240

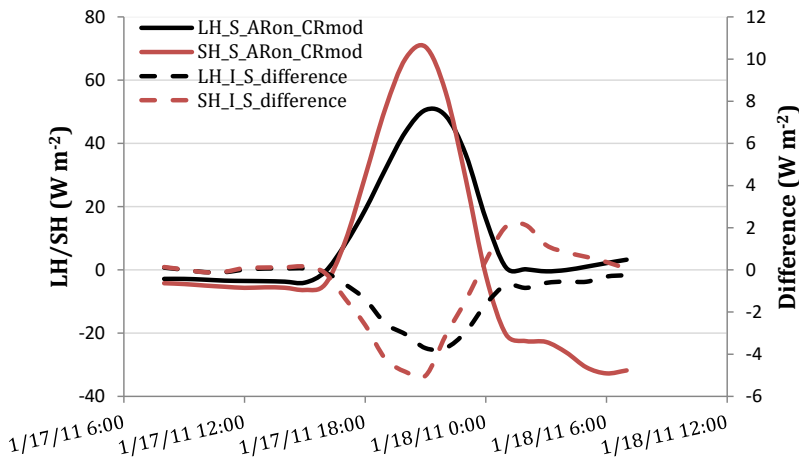
1241

1242
1243 Figure 12. Relative change $((\text{internally mixed} - \text{source-oriented}) / \text{source-oriented} * 100\%)$ in
1244 the daytime averaged predictions during 16 to 18 January 2011 for (a) the ratio of cloud
1245 liquid water mixing ratio, (b) cloud droplet number and absolute difference (internally mixed
1246 - source-oriented) in (c) surface skin temperature (K) and (d) net shortwave radiation (W m^{-2}). (a) and (b) are average values using data within the first five model layers. Contours are
1247 terrain heights in m.
1248

1249
1250
1251
1252



1253



1254
1255
1256
1257
1258

Figure 13. Area average of latent heat flux (LH) and sensible heat flux (SH) over the Central Valley in S_ARon_CRmod and the average difference between I_ARon_CRmod and S_ARon_CRmod from 0800 UTC 17 January (00 Z local time) to 0700 UTC 18 January (23 Z local time).